1-1-2015

Towards Closed-Loop Deep Brain Stimulation: Behavior Recognition from Human STN

Soroush Niketeghad
University of Denver

Towards
Closed-loop Deep Brain Stimulation:
Behavior Recognition from Human STN

A Thesis
Presented to
the Faculty of Daniel Felix Ritchie School of Engineering and Computer Science
University of Denver

In Partial Fulfulment
of the Requirements of the Degree
Master of Science

by
Soroush Niketeghad
August 2015
Advisor: Mohammad H. Mahoor

Author: Soroush Niketeghad
Title: Closed-loop Deep Brain Stimulation: Behavior Recognition from Human STN
Advisor: Mohammad H. Mahoor
Degree Date: August 2015

Abstract

Deep brain stimulation (DBS) provides significant therapeutic benefit for movement disorders such as Parkinson's disease (PD). Current DBS devices lack real-time feedback (thus are open loop) and stimulation parameters are adjusted during scheduled visits with a clinician. A closed-loop DBS system may reduce power consumption and side effects by adjusting stimulation parameters based on patient's behavior. Thus behavior detection is a major step in designing such systems. Various physiological signals can be used to recognize the behaviors. Subthalamic Nucleus (STN) Local field Potential (LFP) is a great candidate signal for the neural feedback, because it can be recorded from the stimulation lead and does not require additional sensors. This thesis proposes novel detection and classification techniques for behavior recognition based on deep brain LFP. Behavior detection from such signals is the vital step in developing the next generation of closed-loop DBS devices.

LFP recordings from 13 subjects are utilized in this study to design and evaluate our method. Recordings were performed during the surgery and the subjects were asked to perform various behavioral tasks. Various techniques are used understand how the behaviors modulate the STN. One method studies the time-frequency patterns in the STN LFP during the tasks. Another method measures the temporal inter-hemispheric connectivity of the STN as well as the connectivity between STN and Pre-frontal Cortex (PFC). Experimental results demonstrate that different behaviors create different modulation patterns in STN and it's connectivity. We use these patterns as features to classify behaviors.

A method for single trial recognition of the patient's current task is proposed. This method uses wavelet coefficients as features and support vector machine (SVM) as the classifier for recognition of a selection of behaviors: speech, motor, and random. The proposed method is 82.4% accurate for the binary classification and 73.2% for classifying three tasks. As the next step, a practical behavior detection method which asynchronously detects behaviors is proposed. This method does not use any priori knowledge of behavior onsets and is capable of asynchronously detect the finger movements of PD patients. Our study indicates that there is a motor-modulated inter-hemispheric connectivity between LFP signals recorded bilaterally from STN. We utilize a non-linear regression method to measure this inter-hemispheric connectivity and to detect the finger movements. Our experimental results using STN LFP recorded from eight patients with PD demonstrate this is a promising approach for behavior detection and developing novel closed-loop DBS systems.

Acknowledgements

I would like to express my deepest gratitude to my advisor Dr. Mohammad Mahoor and my co-advisor Dr. Adam Hebb for giving me an opportunity to work on this project and for their constant guidance and support. Special thanks to Dr. Sara Hanrahan and Joshua Nedrud from Colorado Neurological Institute (CNI) for the LFP data recording and their constructive support for signal analysis. I would also like to thank thesis committee members, Dr. Ali Besharat, Dr. Bradly Davidson, and Dr. Jun Zhang.

I want to thank my parents for their selfless support. Without their help I would not accomplish the goals of this project. I want to appreciate all my lab mates who gave me tremendous courage and motivation to complete this research. Also many thanks to the University of Denver administrators and faculty who provided me a productive academic environment and fascinated my study at DU.

This research was partially supported by a grant from the Knoebel Institute for the Longevity and Health at University of Denver and I like to thank them for their financial support.

Contents

Abstract **ii**

Acknowledgements **iii**

List of Figures **vii**

List of Tables **xi**

Abbreviations **xii**

1 Introduction **1**
1.1 Parkinson's Disease 1
1.2 Deep Brain Stimulation 2
1.3 Closed-loop DBS 6
1.4 Thesis Goals and Impacts 6
1.4.1 Thesis Contribution and Road Map 8

2 Data Recording **10**
2.1 Subjects 10
2.2 DBS Surgery and Recording Design 10
2.3 Behavioral Study 14

3 Task related modulations and Interconnections **15**
3.1 Background 15
3.2 Modulation of Beta Oscillatory Activity During Movement and Speech Tasks 16
3.2.1 Brain waves 16
3.2.1.1 Delta waves (.5 to 3 Hz) 17
3.2.1.2 Theta waves (3 to 8 Hz) 17
3.2.1.3 Alpha waves (8 to 12 Hz) 17
3.2.1.4 Beta waves (12 to 38 Hz) 18
3.2.1.5 Gamma waves (38 to 42 Hz) 18
3.2.2 Methods of Time-Frequency Analysis 19

3.3 Bilateral Interconnection of STN and STN-PFC During Movement and Speech Tasks . . . 20
3.3.1 Background . . . 20
3.3.2 Methods of Measuring Connectivity . . . 22
3.3.2.1 Preprocessing . . . 22
3.3.2.2 Obtaining the Phases . . . 23
3.3.2.3 Calculating the PLV . . . 24
3.3.3 Statistics . . . 24
3.4 Experimental Results . . . 25
3.4.1 Single channel time-frequency results . . . 26
3.4.2 Task modulated connectivity results . . . 26
3.5 Discussion . . . 27

4 Classification of Behavioral Tasks 45
4.1 Background . . . 45
4.2 Classification Method . . . 46
4.2.1 Preprocessing . . . 46
4.2.2 Feature Extraction . . . 46
4.2.3 Classifier . . . 47
4.3 Experimental results . . . 49
4.3.1 Feature Extraction . . . 49
4.3.2 Classification . . . 49
4.4 Discussion . . . 51

5 Asynchronous Detection of Movement 53
5.1 Background . . . 53
5.2 Detection Method . . . 55
5.2.1 Preprocessing . . . 55
5.2.2 Non-linear Regression . . . 55
5.2.3 Component Selection . . . 57
5.2.4 Template Matching . . . 58
5.2.4.1 Creating the Template . . . 58
5.2.4.2 Real Time Template Matching . . . 58
5.2.5 Determination of Detected Times . . . 59
5.2.6 Evaluation . . . 59
5.3 Experimental Results . . . 59
5.4 Disscussion . . . 62

6 Conclusion, Discussion, and Future Research Direction 67
6.1 Conclusion . . . 67
6.2 Discussion and Future Work . . . 68

Bibliography **71**

Conditional Variance **83**

Component selection **85**

List of Figures

1.1 New Medtronic Activa PC+S IPG and the DBS lead. 3
1.2 The lead for DBS is implanted in either the subyhalamic nucleus or the internal segment of the globus pallidus. The lead passes through a burr hole in the skull. Attached to the lead is a connecting wire, which is tunneled under the skin of the scalp an neck to the anterior chest wall, where it is connected to an impulse generator [1]. 4
1.3 Physician programmer (middle) provides variety of adjustments. Patient programmer (right) controls by the patients and is ablr to turn the stimulation on and off. for the new devices the patients programmer is also ablr to initiate the data recording for limited period of time. 5
1.4 New DBS devices are able to simultaneously record and stimulate. This provides the hardware requirements of implementing a closed-loop DBS device [2]. 7

2.1 Atlas representation DBS lead (A) and demonstrating pME (B) in dorsal STN (yellow) [3]. 12
2.2 Schematic representation of recording electrodes used for LFP recordings. (A) Medtronic 3389 DBS lead. (B) Alpha Omega neuroprobe microelectrode. Recordings were obtained from the labeled reference contact [3]. 13

3.1 Main circuits of the basal ganglia. Picture shows 2 coronal slices that have been superimposed to include the involved basal ganglia structures. + and - signs at the point of the arrows indicate respectively whether the pathway is excitatory or inhibitory in effect [4]. 29
3.2 Comparison among single neuron (spike) recording, local field potentials and Surface EEG. [5]. 30
3.3 Spectrum of brain waves from high frequency (Gamma) to low frequency (Delta) [6] 30

3.4 Communication between neuronal populations through phase synchronization. Spikes that arrive at excitability periods of the receiving neuronal group have pointed arrowheads. Spikes that miss excitability periods have blunt arrowheads. The red and green neuronal groups undergo coherent excitability fluctuations and their communication is therefore effective. The black neuronal group however undergoes excitability fluctuations that are not coherent with the green neuronal group and therefore communication between the green and the black neuronal group is prohibited [7]. 31
3.5 Segments of data for each trial were extracted based on the recorded Audio or EMG for speech and finger movement tasks respectively. 32
3.6 Complex wavelet transform uses complex wavelets with different scales to decompose the signal into different frequency components. 33
3.7 For each data point, the phase of the complex value is obtained to form a sequence of phases. 33
3.8 Procedure of calculating phase locking values. The phase difference between two channels (STN LFP and PFC ECoG) are calculated. Phase differences are averaged over trials and their absolute values are calculated as the plv of the channels. 34
3.9 PLVs are segmented into time-frequency windows of size 0.5 Hz by 200 ms. 34
3.10 Spectral power corresponding to alpha and beta range for subject 5 are suppressed around 500 ms before the speech task onset (0s) and lasts until the task offset (6s). 35
3.11 Spectral power corresponding to high alpha and low beta range for subject 1 are suppressed around 500 ms before the speech task onset (0s) and lasts until the task offset (6s). 36
3.12 Spectral power corresponding to theta, alpha and beta range for subject 5 are suppressed around 500 ms before the speech task onset (0s) and is followed by a significant augmentation 1s after onset. 37
3.13 Spectral power corresponding to alpha and low beta range for subject 1 are suppressed around 500 ms before the speech task onset (0s) and is followed by a significant augmentation 1s after onset. 38
3.14 Described task modulated pattern for speech in subject 3 is significant in channel 3 while channels 4-6 demonstrate random task independent fluctuations. 39
3.15 Described task modulated pattern for finger movement in subject 3 is significant in channel 2 while channels 4 and 5 demonstrate random task independent fluctuations. 40
3.16 Single trial spectral power corresponding to alpha and beta range for subject 1 for speech trial. 40
3.17 Single trial spectral power corresponding to alpha and low beta range for subject 1 for finger movement trial. 41

3.18 Spectrograms of PLVs across 6 LFP channels implanted in right and left STN for speech task. In the spectrogram resulting from the connectivity of second right channel and third left channel a significant synchronization can be observed around 4 Hz during the speech task. 41
3.19 Spectrograms of PLVs across 6 LFP channels implanted in right and left STN for motor task. In the spectrogram resulting from the connectivity of third right and second left channels as well as third right and third left channels, significant synchronizations can be observed around 4 Hz during the motor task. 42
3.20 Spectrograms of PLVs across 6 LFP channels Vs. 3 ECoG channels implanted in right and left STN as well as PFC for speech task. In the spectrogram resulting from the connectivity of third right LFP channel and second ECoG channel, a significant synchronization can be observed around 4 Hz during the speech task. 43
3.21 Spectrograms of PLVs across 6 LFP channels Vs. 3 ECoG channels implanted in right and left STN as well as PFC for speech task. In the spectrogram resulting from the connectivity of third right LFP channel and second ECoG channel, a significant synchronization can be observed around 4 Hz during the speech task. 44

4.1 SVM uses risk optimization to compare various separating hyperplanes and chooses the model with the largest margin of separation [8]. 48
4.2 Time-frequency window selected for extracting the features. Each window starts from half a second before onset and lasts for 4 seconds.and contains freqiency components corresponding to 8-30 Hz. 50
4.3 Three class classification results for linear and RBF kernel SVM. 51

5.1 (a) LFP data are recorded from all four channels of each DBS lead located in each hemisphere. (b) Signals are bipolar re-referenced and downsampled. (c) Intercorrelation between each bilateral pair of channels is measured as $h^{2*}_{XY}[n]$ (total of 9 pairs). (d) A linear combination of channels is selected using PCA. (e) Correlation between $h^{2*}_{XY}[n]$ and the template is calculated to derive the feature vector $\gamma^{2*}_{XY}[n]$. (f) Single events are detected by thresholding the values of $\gamma^{2*}_{XY}[n]$. 56
5.2 Time windowing of two channels for non-parametric non-linear regression analysis. 57
5.3 A segment of labels generated from the digital channel (a) and scores created by the algorithm (b). a threshold of 0.68 is considered for event detection and the samples are labeled as TP, FP, TN, FN based on their score $\gamma^{2*}_{XY}[n]$, threshold θ and the corresponding label sample $ev[n]$. 60
5.4 Templates created from the first trial block for each subject by averaging all the 15 trials. The templates are 3 seconds long starting from 1.5 seconds before the trial onset. The values are normalized and are between 0 and 1. . 61

5.5 Templates corresponding to the speech and motor task for subject 3. For motor tasks the templates starts 1.5 seconds before the onset and lasts 3 seconds. For the speech task the template starts 3 seconds before the onset and ends one second after the maximum offset among the trials. The values are normalized and are between 0 and 1. the missing points are Nan values created by division by zero. 62

5.6 ROC curves generated for eight subjects. x axis corresponds to the false positive rate (FPR) and y axis corresponds to the true positive rate (TPR) as explained in Section 5.2.6. The ROC curves generated in a leave-one-block-out technique are interpolated and averaged over the iterations to produce these results. The solid line demonstrates the proposed detector performance where any point on the line can be achieved by a certain threshold. The dashed line curve represents the performance of the same technique; but instead of component selection a pre-determined pair of bilateral channels that produced the highest performance is selected. The diagonal dotted line represents the performance of a random detector where every sample is either assigned event or nonevent by a uniform binary random function. 66

1 Regression function estimated from the points corresponding to the 2-channel data. 84

List of Tables

2.1 Subject characteristics. All subjects are diagnosed with PD. 11
2.2 Research recording 12
2.3 Amplifiers recording properties 13

4.1 Averaged percentage of classification accuracies for SVM and KNN classifiers 50

5.1 Confusion matrix 60
5.2 The values of true positive rate (TPR) for three different false positive rate (FPR) values as well as area under the curve (AUC) for all subjects. 63

Abbreviations

DBS	**D**eep **B**rain **S**timulation
IPG	**I**mplantable **P**ulse **G**enerator
PD	**P**arkinson's **D**isease
LFP	**L**ocal **F**ield **P**otential
STN	**S**ub**T**halamic **N**ucleus
PFC	**P**re-**F**rontal **C**ortex
EEG	**E**lectro**E**ncephalo **G**ram
ECoG	**E**lectro**Co**rtico **G**ram
EMG	**E**lectro**M**yo **G**ram
BCI	**B**rain **C**omputer **I**nterface
SVM	**S**upport **V**ector **M**achine
KNN	**K**-**N**earest **N**eighbor
PCA	**P**rincipal **C**omponent **A**nalysis

Chapter 1

Introduction

1.1 Parkinson's Disease

Parkinson's disease (PD) is a chronic and progressive movement disorder, meaning that symptoms continue and worsen over time. Nearly one million people in the US are living with Parkinson's disease. The cause is unknown, and although there is presently no cure, there are however treatment options such as medication, surgery and deep brain stimulation to manage its symptoms.

Parkinsons involves the malfunction and death of vital nerve cells in the brain, called neurons. Parkinson's primarily affects neurons in the an area of the brain called the substantia nigra [9]. Some of these dying neurons produce dopamine, a chemical that sends messages to the part of the brain that controls movement and coordination [10]. As PD progresses, the amount of dopamine produced in the brain decreases, leaving a person unable to control movement normally.

The specific group of symptoms that an individual experiences varies from person to person. Primary motor signs of Parkinsons disease include the following:

- tremor of the hands, arms, legs, jaw and face

- bradykinesia or slowness of movement
- rigidity or stiffness of the limbs and trunk
- postural instability or impaired balance and coordination

Scientists are also exploring the idea that loss of cells in other areas of the brain and body contribute to Parkinsons. For example, researchers have discovered that the hallmark sign of Parkinsons disease clumps of a protein alpha-synuclein, which are also called Lewy Bodies are found not only in the mid-brain but also in the brain stem and the olfactory bulb.

These areas of the brain correlate to nonmotor functions such as sense of smell and sleep regulation. The presence of Lewy bodies in these areas could explain the nonmotor symptoms experienced by some people with PD before any motor sign of the disease appears. The intestines also have dopamine cells that degenerate in Parkinsons, and this may be important in the gastrointestinal symptoms that are part of the disease.

1.2 Deep Brain Stimulation

Deep brain stimulation (DBS) is a therapy including a surgical procedure for treating several neurological disorders most commonly the debilitating motor symptoms of PD, mentioned in 1.1. The procedure is also used to treat essential tremor [11, 12] and dystonia [13, 14]. DBS is used only for patients whose symptoms cannot be sufficiently controlled with medications. However, only patients who a certain degree of improvement after taking medication for Parkinsons benefit from DBS. DBS uses a surgically implanted, battery-operated medical device called an implantable pulse generator (IPG) - similar to a heart pacemaker and approximately the size of a stopwatch to - deliver electrical stimulation to

specific areas in the brain that control movement, thus blocking the abnormal nerve signals that cause PD symptoms (Figure 1.1).

FIGURE 1.1: New Medtronic Activa PC+S IPG and the DBS lead.

Before the procedure, a neurosurgeon uses magnetic resonance imaging (MRI) or computed tomography (CT) scanning to identify and locate the exact target within the brain for surgical implantation [15, 16]. Some surgeons may use microelectrode recording - which involves a small wire that monitors the activity of nerve cells in the target area - to more specifically identify the precise brain area that will be stimulated [17]. Generally, these areas are the thalamus, subthalamic nucleus, and globus pallidus. There is a low chance that placement of the stimulator may cause bleeding or infection in the brain.

The DBS system consists of three components: the lead, the extension, and the IPG (Figure 1.2). The lead (also called an electrode)a thin, insulated wireis inserted through a small opening in the skull and implanted in the brain. The tip of the electrode is positioned within the specific brain area.

The extension is an insulated wire that is passed under the skin of the head, neck, and shoulder, connecting the lead to the implantable pulse generator. The IPG (the "battery

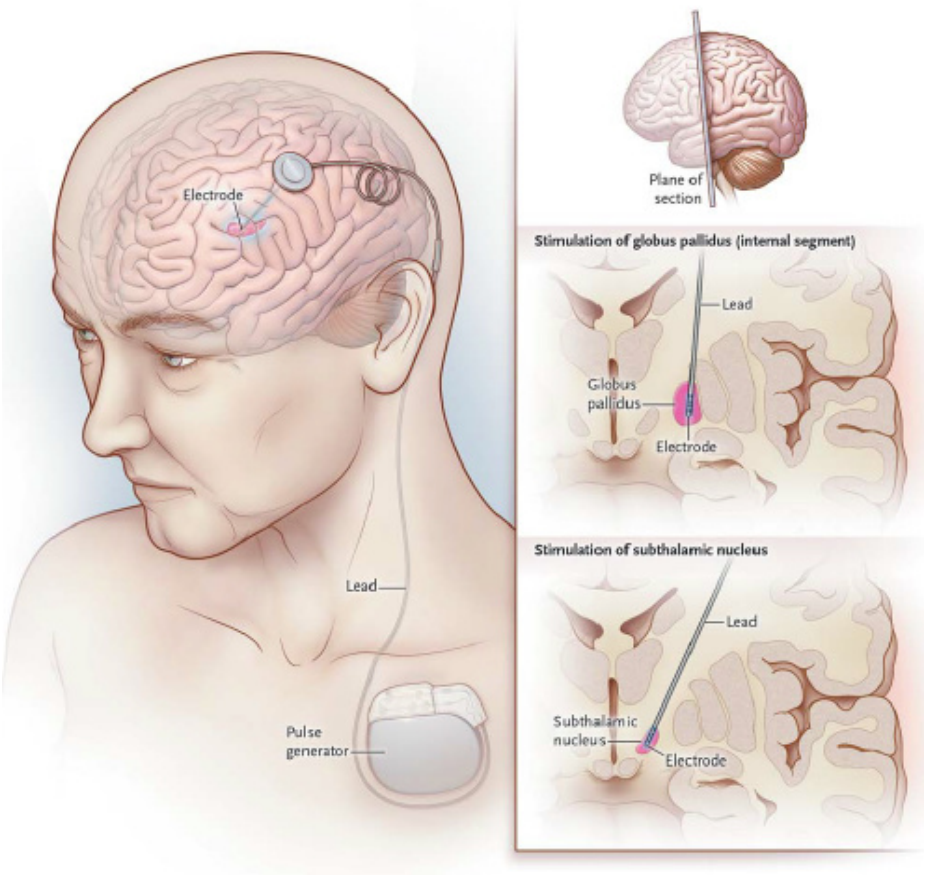

FIGURE 1.2: The lead for DBS is implanted in either the subyhalamic nucleus or the internal segment of the globus pallidus. The lead passes through a burr hole in the skull. Attached to the lead is a connecting wire, which is tunneled under the skin of the scalp an neck to the anterior chest wall, where it is connected to an impulse generator [1].

pack") is the third component and is usually implanted under the skin near the collarbone. In some cases it may be implanted lower in the chest or under the skin over the abdomen.

Once the system is in place, electrical impulses are sent from the IPG up along the extension wire and the lead and into the brain. These impulses block abnormal electrical signals and alleviate PD motor symptoms.

Comparing to previous surgeries for PD, DBS causes less amount of permanent surgical changes to the brain. Instead, the procedure uses electrical stimulation to regulate electrical signals in neural circuits to and from identified areas in the brain to improve PD

symptoms. Thus, if DBS causes unwanted side effects or newer, more promising treatments develop in the future, the implantable pulse generator can be removed, and the DBS procedure can be halted. Also, stimulation from the IPG is easily adjustable without further surgery if the persons condition changes. Some people describe the pulse generator adjustments as "programming". Parameters like amplitude, frequency and pulse width can be easilly adjusted through the DBS programmers. New generation of DBS devices (Activa PC+S) can be programmed through a radio device in a completely non-invasive procedure (Figure 1.3).

FIGURE 1.3: Physician programmer (middle) provides variety of adjustments. Patient programmer (right) controls by the patients and is ablr to turn the stimulation on and off. for the new devices the patients programmer is also ablr to initiate the data recording for limited period of time.

Although most patients still need to take medication after undergoing DBS, many people with Parkinsons disease experience considerable reduction of their motor symptoms and are able to reduce their medications. The amount of reduction varies but can be considerably reduced in most patients, and can lead to a significant improvement in side effects such as dyskinesias (involuntary movements caused by long-term use of levodopa). In

some cases, the stimulation itself can suppress dyskinesias without a reduction in medication [18]. DBS does not improve cognitive symptoms in PD and indeed may worsen them, so it is not generally used if there are signs of dementia [19]. DBS changes the brain firing pattern but does not slow the progression of the neurodegeneration.

1.3 Closed-loop DBS

In order to adapt to the patients' condition, the new generation of DBS systems are redesigned so as to include a closed-loop feedback control where the patients' symptoms are continuously monitored and the stimulation is adapted in response to its variations. To design an adaptively controlled closed-loop DBS system, it is necessary to find a proper physiological signal that can be easily measured and has predictive information on tremor as well as patient's behavioral tasks. One such feedback signal could be the muscular activity measured by means of surface electromyogram (sEMG) and accelerometer (acc) signals can be recorded non-invasively from the patient's symptomatic extremities. Current studies on closed-loop DBS relies on these signals because they are easy to capture and there are many studies on using them for brain computer interfaces (BCI). New DBS systems are designed to simultaneously stimulate and record the LFP signals which provides the opportunity for designing a new generation of closed-loop devices that use the LFP signals as the neural feedback (Figure 1.4).

1.4 Thesis Goals and Impacts

The main goal of this thesis is to provide a method for behavior recognition that will ultimately be used in the next generation of closed-loop DBS devices. The stimulation

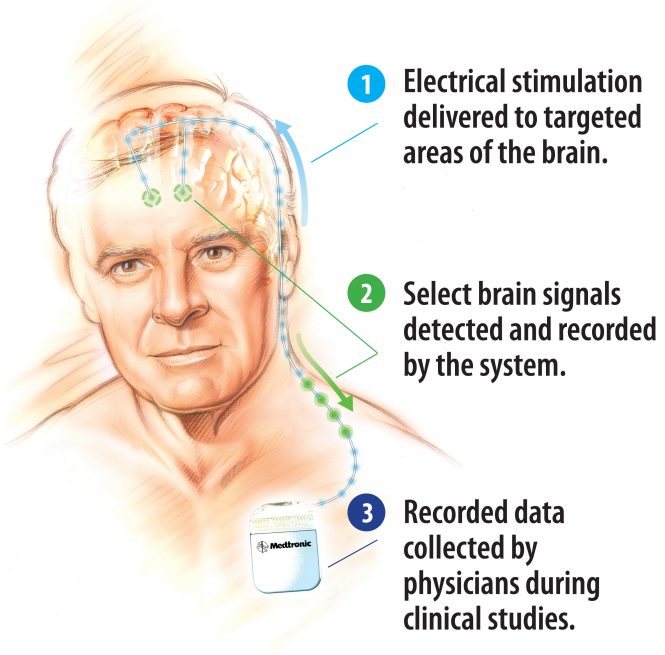

FIGURE 1.4: New DBS devices are able to simultaneously record and stimulate. This provides the hardware requirements of implementing a closed-loop DBS device [2].

parameters can be optimized based on patient's behavioral tasks to deliver the best therapy with the least side effects and minimal battery usage.

The superiority of a closed-loop DBS system to the current open-loop DBS devices is due to the fact that delivering short time stimulation pulses in the right time is proven to have similar therapeutic effects compared to continuous stimulation. In addition, it dramatically decreases the battery usage and temporary side effects [20]. The advantage of the proposed behavioral level closed-loop DBS system is that for some specific behaviors such as initiating the speech, the stimulation can be problematic and hence the proposed device is able to recognize the task initiation and apply proper adjustments.

In order to design a behavioral level closed-loop DBS device the following research aims should be addressed:

- How the information provided by the LFP signals recorded from the stimulation lead can be decoded to behavioral tasks?

- What mapping techniques can provide the optimum stimulation parameters based on the decoded behaviors?

In this thesis we address the first research aim. Our contribution to this aim includes analyzing the LFP signals and deep brain connectivities and subsequently using these analyses to find meaningful features for classification and detection of behaviors.

1.4.1 Thesis Contribution and Road Map

- Two novel data sets of LFP recordings are used in this thesis for design and evaluation of our method. The first dataset was recorded at the University of Washington and the second one has been recorded in Colorado Neurological Institute (CNI) during this research. Recordings were performed during the surgery and subjects were asked to perform various behaviors such as speech and finger movement. Chapter 2 describes the data set and the recording paradigms.

- In Chapter 3 we analyze the LFP and ECoG data recorded from the patients with PD to characterized the signals during behavioral tasks performances. Our analysis also includes investigating the temporal connectivity between the right and left STN as well as between the STN and Prefrontal Cortex (PFC).

- Subsequently in Chapter 4, we use the analysis to identify suitable features for decoding behaviors. Using the time-frequency patterns of different behaviors we are able to classify the segments of LFP signals associated with three different behaviors: speech, finger movement and rest.

- Since a real time closed-loop systems requires detection of self-driven spontaneous tasks, in Chapter 5 we take our approach forward to design an asynchronous event detector. We use a temporal connectivity approach (nonlinear regression) to develop a

novel asynchronous event detection technique. We then present the result of evaluating our proposed algorithm using the LFP signals recorded from a cohort of subjects who have bilaterally implanted DBS leads.

- We conclude the thesis in Chapter 6 with further discussion and directions for future research.

Chapter 2

Data Recording

2.1 Subjects

Thirteen subjects (Table 2.1) undergoing DBS as standard of care for treatment of idiopathic PD were enrolled in this study. All subjects provided informed consent for participation in this research study, in a manner approved by the internal review board (IRB) of the University of Washington and HealthOne. Eighteen independent recordings/lateralities were measured from the thirteen participants. Two subjects underwent sequential recordings from each side, eight had simultaneous bilateral recording, and another two subjects were recorded with a second electrode design and amplifier system in the same hemisphere. There were 8 left, 2 right, and 8 simultaneous bilateral recordings (16 left and 10 right), for a total of 18 recordings for analysis (Table 2.2).

2.2 DBS Surgery and Recording Design

Subjects underwent DBS surgery per clinical routine. All subjects were in the off medication state. Surgery was performed with a Leksell (Elekta, Sweden) stereotactic head

TABLE 2.1: Subject characteristics. All subjects are diagnosed with PD.

Subject	Gender	Age
2	Female	51
3	Female	54
4		
5		
6	Male	63
7	Male	47
8	Male	53
9	Male	58
10	Male	64
11	Female	63
12	Male	70
13	Male	68

frame and Medtronic (Minneapolis, MN, USA) Frame link targeting software. Targeting of the dorsolateral STN was based on a combination of formula based and indirect coordinates. Microelectrodes were positioned in the center and posterior positions of a BenGun trajectory guide, with a parallel separation of 2 mm.

LFP recording was carried out using paired microelectrodes or the DBS lead, or both sequentially (Figure 2.1). For the paired microelectrode (pME) design, we recorded from the macro ring electrodes (reference contact, Figure 2.2) of a pair of dual-channel microelectrodes (Alpha Omega, Israel). The macro ring electrode is stainless steel, has a surface area of 2.2 mm^2 and impedance of 3.2$k\Omega$ (mean; 95% CI = 1.7 - 4.8 $k\Omega$).

Although subjects may have had residual effects from propofol during the initial MER through thalamic nuclei, we did not proceed with recording in the STN region until patients were fully awake and conversant. All research recordings were obtained after clinician testing for proprioceptive modulation of firing rates had begun.

After optical isolation and amplification (MicroGuide, Alpha Omega, Nazareth, Israel), the signals were digitized (4 kHz) and combined with event markers and subject

TABLE 2.2: Research recording

Rec. No.	Sub. No.	Side	Electrode	Amp	Channels		
					Left	Right	ECoG
1	1	Bi	Medtronic DBS lead	SynAMPS2	4	4	4
2	2	Bi	Medtronic DBS lead	SynAMPS2	4	4	8
3	3	Lt	Alpha Omega pME	MicroGuide	1	0	4
4	3	Lt	Medtronic DBS lead	SynAMPS2	4	0	4
5	4	Bi	Medtronic DBS lead	SynAMPS2	4	4	0
6	5	Bi	Medtronic DBS lead	SynAMPS2	4	4	4
7	5	Lt	Alpha Omega pME	MicroGuide	1	0	4
8	6	Lt	Alpha Omega pME	MicroGuide	1	0	4
9	6	Lt	Medtronic DBS lead	SynAMPS2	4	0	4
10	7	Lt	Alpha Omega pME	MicroGuide	1	0	4
11	7	Rt	Alpha Omega pME	MicroGuide	0	1	2
12	8	Lt	Medtronic DBS lead	SynAMPS2	4	0	4
13	9	Lt	Alpha Omega pME	MicroGuide	1	0	4
14	9	Rt	Alpha Omega pME	MicroGuide	0	1	4
15	10	Bi	Medtronic DBS lead	g.USBamp	4	4	0
16	11	Bi	Medtronic DBS lead	g.USBamp	4	4	0
17	12	Bi	Medtronic DBS lead	g.USBamp	4	4	0
18	13	Bi	Boston Sc. DBS Lead	g.USBamp	8	8	0

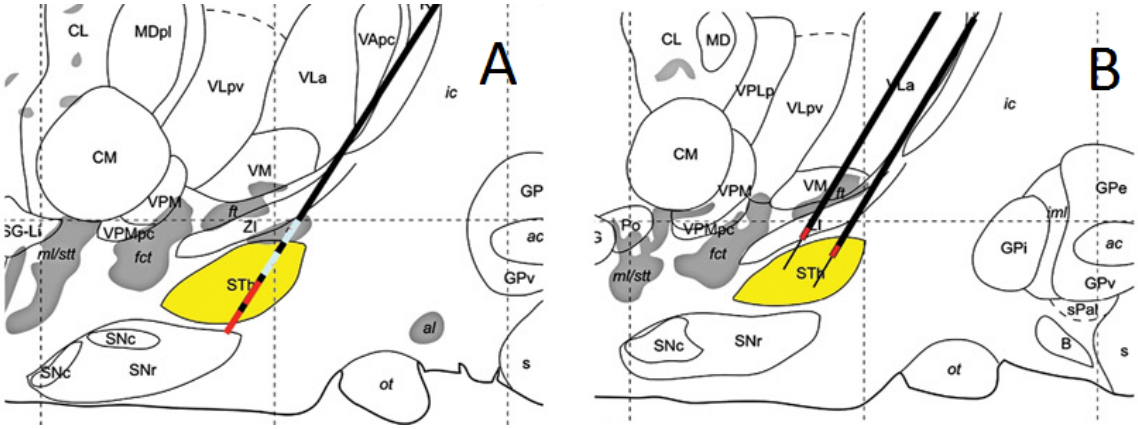

FIGURE 2.1: Atlas representation DBS lead (A) and demonstrating pME (B) in dorsal STN (yellow) [3].

response signals (PowerLab, ADInstruments, New South Wales, Australia). The MER guide tube was used as common reference, and the LFP channels were bipolar re-referenced before analysis.

For the DBS lead recording design, we recorded from each of the four contacts of

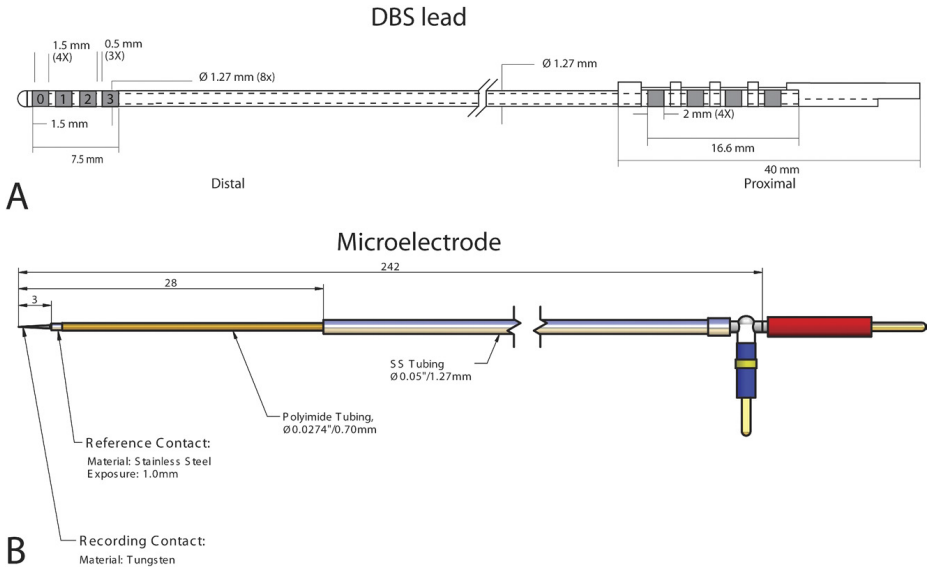

FIGURE 2.2: Schematic representation of recording electrodes used for LFP recordings. (A) Medtronic 3389 DBS lead. (B) Alpha Omega neuroprobe microelectrode. Recordings were obtained from the labeled reference contact [3].

the DBS lead (Medtronic 3389, see Figure 2.2). The DBS lead contact is platinum/iridium, has a surface area of 6.0 mm^2 and impedance of 1.7 $k\Omega$ (mean; 95% CI = 1.1 2.4 $k\Omega$). For one subject (subject 13) recording was performed using Boston Scientific DB-2201-45BC; however there is no sketch available for this lead. Although primarily designed for stimulation, these electrodes have been used for LFP recording in humans, as it does not require modification of standard surgical practice, for example, see [21]. Signals were amplified, digitized (5 kHz), and combined with event markers and subject response signals (SynAMPS2, Neuroscan, Victoria, Australia). A linked mastoid common reference was used for recording, and the LFP channels were subsequently bipolar re-referenced (0-1, 1-2, 2-3) before analysis (see Table 2.3 for more information).

TABLE 2.3: Amplifiers recording properties

Amplifier	Fs (Hz)	Band pass (Hz)
MicroGuide	4000	5 - 300
SynAMPS2	5000	1 - 1000
g.USBamp	4800	0.5 - 2000

2.3 Behavioral Study

Behaviors included motor, speech, and combination tasks. The motor task block consists of 15 cued repetitions of a button press using either the left or right thumb. There are four variants of a speech initiation task: naming the months of the year, counting upward from one, naming the months of the year with a simultaneous button press marking the first month, counting with a simultaneous button press marking the first number. To determine if there was an effect with silent speech, two subjects repeated the naming tasks, but only with mental rehearsal of speech. Speech tasks were also completed in a block of 15 repetitions. On completion of a full set of speech and motor blocks, the entire paradigm was repeated as a second set of blocks in identical order. For task initiation and completion, subjects received an audio cue from a presentation laptop computer running E-Prime 2.0 (Psychology Software Tools, Sharpsburg, PA). A random time factor was programmed into task length to reduce any effect of anticipation.

Chapter 3

Task related modulations and Interconnections

In this chapter, the LFP data recorded from STN is studied through two different approaches. First, the data recored by each contact is studied independently in the time-frequency domain. In another approach, connectivity of the data recorded from two hemispheres are measured and analyzed. Both approaches try to investigate the transient patterns in the basal ganglia created by behavioral tasks.

3.1 Background

In recent years, there has been remarkable studies on how basal ganglia process information [22]. Various findings point out an unexpected role for basal ganglia in the contextual analysis of the environment and using it for planning intelligent behaviors. Cerebral cortex sends the received information to the basal ganglia, and the outputs either return to the frontal cortex or the motor systems in the midbrain and the hindbrain (Figure 3.1). Various areas of cerebral cortex converge upon regions of striatum that, via pallidum and

thalamus return back to the frontal cortex. There is also a less direct pathway from the striatum via the external palidum and STN, and there is a shorter route from thalamus to striatum that bypasses the cerebral cortex. In this thesis we only focus on STN and Prefrontal Cortex (PFC) and their participation in different behavioral tasks as there are a few studies showing that STN particularly involves in generating meaningful speech [23] and movement [24].

Recording of local field potentials (LFP) through bilaterally implanted electrodes in the basal ganglia as well as ECoG recordings from PFC provided a unique research tool for this study. The LFP is the electric potential recorded in the extracellular space in brain tissue, typically using micro-electrodes (metal, silicon or glass micropipettes). LFPs differ from the electroencephalogram (EEG), which is recorded at the surface of the scalp, and with macro-electrodes. It also differs from the electro-corticogram (EcoG), which are recorded from the surface of the brain using large subdural electrodes, while LFPs are recorded in depth, from within the cortical tissue (or other deep brain structures)(Figure 6).

3.2 Modulation of Beta Oscillatory Activity During Movement and Speech Tasks

Basal ganglia and STN rhythms are modulated by behaviors by changing the amplitude (or power) of their oscillations [3, 25]. Time-frequency analysis of LFP recorded from human STN revealed the suppression of β (13-30 Hz) frequency spectral power during motor tasks meaning that beta oscillations are relatively synchronized during the rest state and desynchronized with activity [26, 27].

3.2.1 Brain waves

Brainwaves are divided into bandwidths to describe their functions (below), but are best thought of as a continuous spectrum of consciousness; Delta being slow, loud and functional - to Gamma being fast, subtle, and complex. our brainwaves change according to what we are doing and feeling. When slower brainwaves are dominant we can feel tired, slow, sluggish, or dreamy. The higher frequencies are dominant when we feel wired, or hyper-alert. Brainwave speed is measured in Hertz (cycles per second) and they are dived into bands deliniating slow, moderate, and fast waves 3.3.

3.2.1.1 Delta waves (.5 to 3 Hz)

Delta brainwaves are the slowest but loudest brainwaves (low frequency and deeply penetrating, like a drum beat). They are generated in deepest meditation and dreamless sleep. Delta waves suspend external awareness and are the source of empathy. Healing and regeneration are stimulated in this state, and that is why deep restorative sleep is so essential to the healing process.

3.2.1.2 Theta waves (3 to 8 Hz)

Theta brainwaves occur most often in sleep but are also dominant in the deep meditation. It acts as our gateway to learning and memory. In theta, our senses are withdrawn from the external world and focused on signals originating from within. It is that twilight state which we normally only experience fleetingly as we wake or drift off to sleep. In theta we are in a dream; vivid imagery, intuition and information beyond our normal conscious awareness. Its where we hold our stuff, our fears, troubled history, and nightmares. Alpha waves (8 to 12 Hz)

3.2.1.3 Alpha waves (8 to 12 Hz)

Alpha brainwaves are dominant during quietly flowing thoughts, and in some meditative states. Alpha is the power of now, being here, in the present. Alpha is the resting state for the brain. Alpha waves aid overall mental coordination, calmness, alertness, mind/body integration and learning.

3.2.1.4 Beta waves (12 to 38 Hz)

Beta brainwaves dominate our normal waking state of consciousness when attention is directed towards cognitive tasks and the outside world. Beta is a fast activity, present when we are alert, attentive, engaged in problem solving, judgment, decision making, and engaged in focused mental activity. Beta brainwaves are further divided into three bands; Low Beta (Beta1, 12-15Hz) can be thought of as a 'fast idle, or musing. Beta (aka. Beta2, 15-22Hz) as high engagement. Hi-Beta (Beta3, 22-38Hz) is highly complex thought, integrating new experiences, high anxiety, or excitement. Continual high frequency processing is not a very efficient way to run the brain, as it takes a tremendous amount of energy.

3.2.1.5 Gamma waves (38 to 42 Hz)

Gamma brainwaves are the fastest of brain waves (high frequency, like a flute), and relate to simultaneous processing of information from different brain areas. It passes information rapidly, and as the most subtle of the brainwave frequencies, the mind has to be quiet to access it. Gamma was traditionally dismissed as 'spare brain noise' until researchers discovered it was highly active when in states of universal love, altruism, and the higher virtues. Gamma rhythms modulate perception and consciousness, disappearing under anaesthesia. Gamma is also above the frequency of neuronal firing, so how it is

generated remains a mystery. The presence of Gamma relates to expanded consciousness and spiritual emergence.

3.2.2 Methods of Time-Frequency Analysis

There are generally two approaches for creating time-frequency spectrum of a signal: Short Time Fourier Transform (STFT) and Continuous Wavelet Transform (CWT). STFT applies Fourier transform to time windows that slide through the whole data [28]. Fourier transform calculates the frequency spectrum of the data located in a window and sliding the window adds time dimension to the spectrum:

$$STFT\{x[n]\}(m,\omega) \equiv X(m,\omega) = \sum_{n=-\infty}^{\infty} x[n]w[n-m]e^{-j\omega n} \tag{3.1}$$

where $w[n-m]$ is the sliding window that moves over time by changing the values of n from $-\infty$ to ∞.

On the other hand wavelet transform creates the time and frequency dimensions by sliding and scaling the wavelets respectively [29]:

$$Y_W(c,\tau) = \frac{1}{\sqrt{c}} \int_{-\infty}^{\infty} y(k).\Psi(\frac{t-\tau}{c})dt \tag{3.2}$$

where c is scaling factor, τ represents time shift factor and the wavelet transformation corresponds to a convolution of a function $y(t)$ and a wavelet function. In this study we used the complex Morlet wavelet (`cmor` function in Matlab) and then used the absolute value of the results. A complex Morlet wavelet is defined by [30]:

$$\Psi(t) = \frac{1}{\pi f_b} e^{j2\pi f_c t} e^{\frac{x^2}{f_b}} \tag{3.3}$$

where f_b is a bandwidth parameter and f_c is a wavelet center frequency. In this study we used the values of 1 and 1.5 for f_b and f_c respectively.

In this research we chose to use wavelet transform for performing our time-frequency analysis. STFT uses a constant size window for different frequencies. Therefore a short window might not be long enough to bring up the spectral characteristics of low frequency components and on the other hand, a long window reduces the time resolution specially for rapid spectral changes. Wavelets on the other hand provide an adaptive length in a way that low frequency wavelets are long enough for bringing up the frequency characteristics and high frequency wavelets are short enough to track the temporal changes. However STFT might be useful in other applications because it provides more control on the amount of window length.

3.3 Bilateral Interconnection of STN and STN-PFC During Movement and Speech Tasks

3.3.1 Background

Neurons communicate through excitatory and inhibitory synaptic connections which result in a synchronized network [31]. This synchrony causes a rhythmical extracellular field potential that can be measured in different scales from local field potentials (LFP) to electrocorticography (ECoG) and electroencephalography (EEG). Higher amplitudes of the measured signal correspond to the higher amount of excitations or more synchronized excitations for the neurons included in the recording. However due to the non-stationary and noisy nature of brain signals, amplitude cannot be directly related to the excitation of the neurons. On the other hand, oscillatory phase is a more reliable measure for the neurons oscillatory activity because it is less dependent of the noises originated from the recording

device and the non-related neural activities [32]. When there is a correlation between the oscillatory phases of two different regions, There is a high probability that the regions are coupled. In other words one might control the timing of the action potentials of the other which it is called phase synchronization [33].

Phase synchronization as a fundamental neural mechanism supports neural communication and neural plasticity [34]. Neuronal communication is both performed by oscillatory synchronization within the group of neurons sending a message, as well as by coherence (or phase-locking) between the oscillations in the sending group and the receiving group (Figure 3.4) [7]. Activated neuronal groups have the intrinsic property to oscillate [35, 36]. Those oscillations causes excitability fluctuations that do not only affect the output of the neuronal group directly, but also modulates its sensitivity to input [37, 38]. Therefore, oscillations of a neuronal group rhythmically controls (by openning and closing) the group's windows as a relay for communication. As a result that different groups of neurons can only communicate effectively with each other if the rhythmic opening of their communication windows are opened to each other. In the other words, when a sending group wants to communicate effectively to a receiving group, the sending group's output has to be sent a time such that it arrives at the receiving group when that group is excitable.

Synchronization happens in different frequencies for different pairs of regions. For regions that are anatomically located close to each other the synchronization happens in higher frequencies due to the small amount of time required for firings to be communicated. On the other hand, for ergions located anatomically far from each other, synchronization happens in low frequencies due to the relatively long distance that the message should travel to get to the receiving populations.

Synchronization in primary and secondary motor areas is responsible for coordinated

movements in several animal experiments [39]. Theta and upper alpha band synchronization are related to working memory and long term memory process [33, 40]. Phase synchronization has also been observed in pathological activities in epilepsy and Parkinson patients [41, 42]. With a prior knowledge of anatomical connections we supposed there is a hyper direct connectivity between subtalamic nucleus (STN) and prefrontal cortex (PFC). Simultaneous recordings of LFP and ECoG signals during the deep brain stimulation (DBS) electrode implantation surgery provide us a rare opportunity to examine the brain connectivity among STNs of different sides and PFC. Analysis of the LFP signals from bilateral STN demonstrates a synchronization during button pressing tasks [43]. However, there has not been any study of the connectivity between the STN and PFC. This study investigates the event related phase synchronization between the LFP signals of bilateral STN recorded through implanted DBS electrodes and ECoG signals recorded from the PFC.

3.3.2 Methods of Measuring Connectivity

Generally when the phases of two oscillators are synchronized, their rhythms are adjusted so that they are phase-locked. Rosenblum et al. [44] define phase-locking as when two oscillators maintain a constant value for their phase difference. However in neuroscience, due to the noisy nature of brain signals the phase-locking is defined as an approximately constant difference between the phases of two oscillatory signals. Our analysis uses phase-locking statistics [45] to calculate phase-locking values (PLV) among STN of two hemispheres as well as STN Vs. prefrontal cortex (PFC).

3.3.2.1 Preprocessing

LFP and ECoG recordings are bipolar re-referenced by subtracting adjacent contacts (1-0, 2-1, 3-2). This way power line interference (PLI) is removed without any filtering

related distortions. Bipolar re-referencing also removes the compontn of the signal that represents the common brain activity between the two channels. This improves the performance of the algorithms because the common activity is mostly (not completely) is related to the activity from the other regions. In the other words the common activity is more likely unrealted to the task modultaed STN LFP.

An FIR zero-phase filter with transient band of 200-250 Hz (i.e. the frequency response starts decaying at 200 Hz and it reaches to it's minimum at 250 Hz) is applied on data using the `filtfilt` function implemented in Matlab [46]. After applying the anti-aliasing filter, the signals are downsampled to 500Hz. Segments of data for each trial are extracted based on the recorded Audio or EMG for speech and finger movement tasks respectively (see Figure 3.5).

3.3.2.2 Obtaining the Phases

Capturing the phases of time series requires mapping the frequency components into complex domain or in other words computing the analytic signal. In mathematics and signal processing, an analytic signal is a complex-valued function that has no negative frequency components [47]. If $s(t)$ is a real-valued function with Fourier transform $S(f)$, the function

$$S_a(f) \equiv \begin{cases} 2S(f), & \text{for } f > 0 \\ S(f), & \text{for } f = 0 \\ 0, & \text{for } f < 0 \end{cases} \tag{3.4}$$

contains only the non-negative frequency components of $S(f)$. The analytic signal of $s(t)$ is the inverse Fourier transform of $S_a(f)$:

$$s_a(t) \equiv \mathcal{F}^{-1}[S_a](t) = s(t) + j\hat{s}(t) \tag{3.5}$$

where $\hat{s}(t)$ is the Hilbert transform of $s(t)$:

$$\hat{s}(t) \equiv H(s)(t) = -\frac{1}{\pi} \lim_{\epsilon \to 0} \int_{\epsilon}^{\infty} \frac{u(t+\tau) - u(t-\tau)}{\tau} d\tau \tag{3.6}$$

For phase extraction, the signal needs to be decomposed into its frequency components and then the analytic signal is calculated for each component. Complex wavelets can provide the analytic signals in a more straight forward procedure. The complex nature of the wavelets maps the real signal to the complex domain. By using wavelets with different scales, we decompose the signal into different frequency components. As a result we obtain a time series of complex numbers for every trial and each frequency component (Figure 3.6).

3.3.2.3 Calculating the PLV

Since we are only interested in the phase synchrony, we created a sequence of the phases from the sequence of the complex numbers (Figure 3.7). The phase difference between the two channels is then calculated and averaged over trials. Higher amplitudes correspond to the phases that maintain an approximately constant value through the trial while randomly distributed phase result is a near zero amplitude in the average. Since we are more interested in the amount of phase locking rather than the specific synchronization phase, the PLV is defined as the absolute value of the averaged phases (Figure 3.8).

3.3.3 Statistics

Permutation (bootstrap) analysis were applied to the time-frequency responses to verify the significance of synchronizations/desynchronizations. Permutation was performed by randomly shuffling the second channel through the trials. This way most likely the PLV corresponding to a pair of signals that are happening in different times is caculated to be compared with the actual PLV. For example, if there are three trials of data, in calculating

the actual PLV phase difference between channel 1 and 2 for each trial is calculated and then is averaged. On the other hand to create a random permutation, for instance phase difference between channel 1 of trial 1 and channel 2 of trial 3 is calculated. Also phase difference of channel 1 of trial 2 and channel 2 of trial 1 as well as channel 1 of trial 3 and channel 2 of trial 2 is calculated. Subsequently these phase differences are averaged to create a permutation.

To correct for multiple comparisons, we segment the data into independent time frequency windows (Figure). The size of these windows is chosen to be 0.5 Hz by 200 ms. Since the length of time-frequency components of speech is 8 seconds and for button pressing is 6 seconds and the interested frequency range is 1-11 Hz, the speech and button pressing tasks require $20 \times 40 = 8000$ and $20 \times 30 = 6000$ multiple comparisons. We calculated the number of bootstraps such that the resolution of our p-value is 2.5 % for the high values and 2.5% for the low values in a two tailed T test. This calculation is $2 \times (2.5\%/8000)^{-1} = 640,000$ and $2 \times (2.5\%/6000)^{-1} = 480,000$ for speech and button pressing tasks respectively. Therefore, after normalizing each PLV segment for each frequency, the sum of values in each time-frequency segment were compared to the corresponding summation in the actual PLV. Next, the insignificant time frequency windows are set to zero. To reduce the sharp edges, a mean filter effect is then applied to the PLVs.

3.4 Experimental Results

The experimental results in this section are divided into single channel time-frequency analysis results and task modulated connectivity results. Since the research presented in this chapter was performed prior to the data recordings at CNI, only the data recorded at the University of Washington are used in this chapter.

3.4.1 Single channel time-frequency results

Using the described continuous wavelet transform, a time-frequency analysis of segments of LFP data correlated with speech and finger movement tasks is performed. All the time-frequency components ate then averaged over trials to reduce noise and event unrelated patterns. Figures 3.10 and 3.11 demonstrates the time-frequency analysis of the speech task for subjects 5 and 1 respectively. Similarly, Figures 3.12 and 3.13 demonstrates the time-frequency analysis of the finger movement task for subjects 5 and 1 respectively. The values demonstrated from blue(-5) to red(+5) are normalized wavelet coefficients over each frequency. LFP recordings corresponding with the speech tasks demonstrate a suppression in alpha and beta (8-30 Hz) powers starting around 500 ms before the task onset and lasting until the task offset (Figure 3.10). The finger movement task creates a similar pattern following with significant augmentation (Figure 3.11). For some subjects the pattern however is limited to the high alpha and low beta (10-15 Hz) (Figure 3.12). The motor pattern extends to theta range for some subjects (4-8 Hz) and for some subjects it does not have high beta components (Figure 3.13).

The pattern created by a subject is limited to certain channels. For some channels the described pattern is significantly observable while for some channels the spectrogram only shows random fluctuations that are independent from the task (Figures 3.14 and 3.15).

To investigate the stability of the LFP data over trials, time-frequency figures corresponding to a single trial for the same subject and channel of Figures 3.11 and 3.13 are illustrated in Figures 3.16 and 3.17.

3.4.2 Task modulated connectivity results

As described in the previous section, the phase locking values calculated for measuring the connectivity of STN in two hemispheres as well as STN Vs. PFC are distributed in

two dimensions (time and frequency). A permutation analysis is applied on the results of phase synchronization to find the statistically significant components in the spectrograms.

Figures 3.18 and 3.19 demonstrates the spectrograms of plv values across 6 LFP channels implanted in right and left STN for speech and motor tasks respectively. In the spectrogram resulting from the connectivity of second right channel and third left channel a significant synchronization can be observed around 4 Hz during the speech task (Figure 3.18). Similarly same synchronization pattern is observed for the motor task significantly between third right and second left channels as well as third right and third left channels (Figure 3.19). The synchronization however does not last as long as it lasted for the speech task.

Synchronization among STN and PFC is demonstrated through 6 LFP and 3 ECoG channels for speech and motor tasks in Figures 3.20 and 3.21 respectively.

3.5 Discussion

A nearly consistent pattern was observed in the time-frequency analysis of speech and finger movement tasks over subjects. LFP recordings corresponding with the speech tasks demonstrate a suppression in alpha and beta (8-30 Hz) powers while the finger movement task creates a similar pattern following with significant augmentation.

Comparing the single trial results (Figures 3.16 and 3.17) to the average time-frequency figures illustrates that there is a significant amount of brain activity that is not related to the events. Therefore the single trial analysis is not able to provide a clear visual illustration of different patterns.

The beta synchronization/desynchronization is related to the oscillation among basal ganglia nuclei. Computational modeling of GPe-STN circuit suggests that the delay between these structures is sufficient to produce beta oscilations [48]. The reason for the event

related beta desynchronization of STN is that neurons responsible for different muscles start firing with different phases to perform that specific task. As a results random firing phases of neurons creates a desynchronization [27].

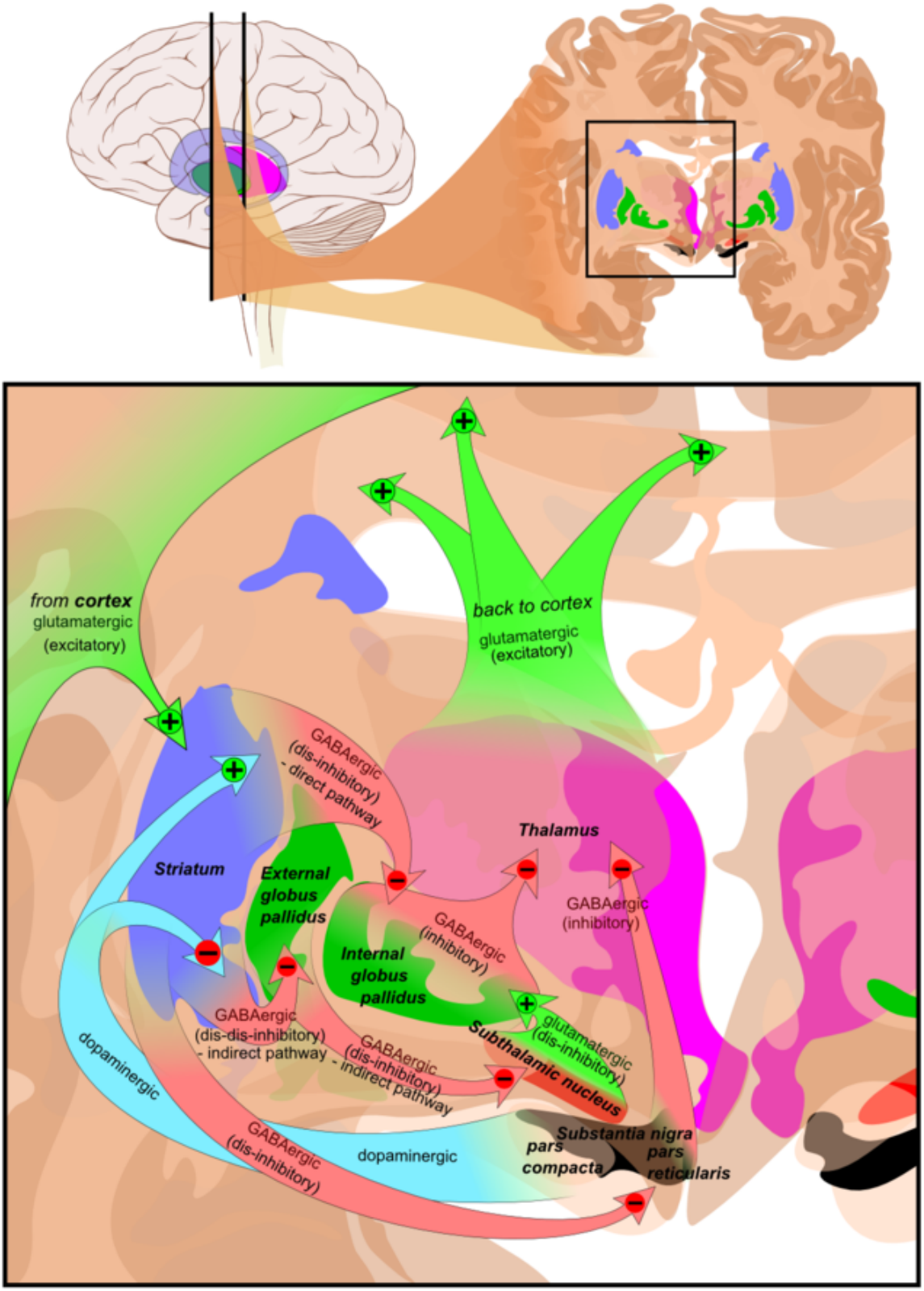

FIGURE 3.1: Main circuits of the basal ganglia. Picture shows 2 coronal slices that have been superimposed to include the involved basal ganglia structures. + and - signs at the point of the arrows indicate respectively whether the pathway is excitatory or inhibitory in effect [4].

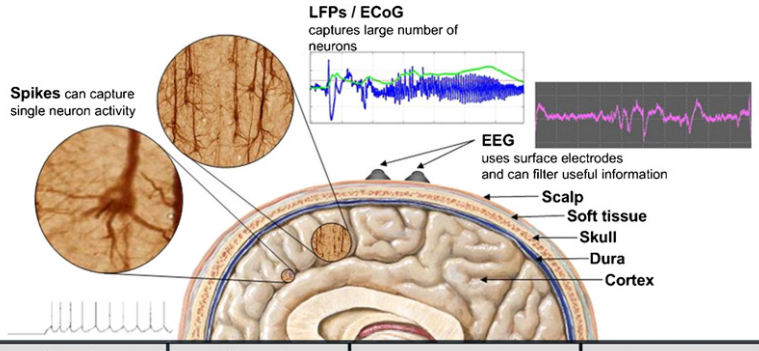

Sensing Methodology	Chronic Recording	Information Coding	System Power
Spike Recording	Challenging Interface Stability	High Fidelity, Need Ensemble Averages for Disease State	High Bandwidth/ Power & Data Processing Req.
Field Potentials	Less Sensitive to Interface Stability, Reuse Existing Technology	Medium Fidelity, Direct Relation to Disease State	Less Bandwidth/ Power & Data Processing Req.
Surface EEG	Irritation High Interference	Lower Fidelity, Less Spatial, Temporal, & Spectral Resolution	External Power Source Can Be Used

FIGURE 3.2: Comparison among single neuron (spike) recording, local field potentials and Surface EEG. [5].

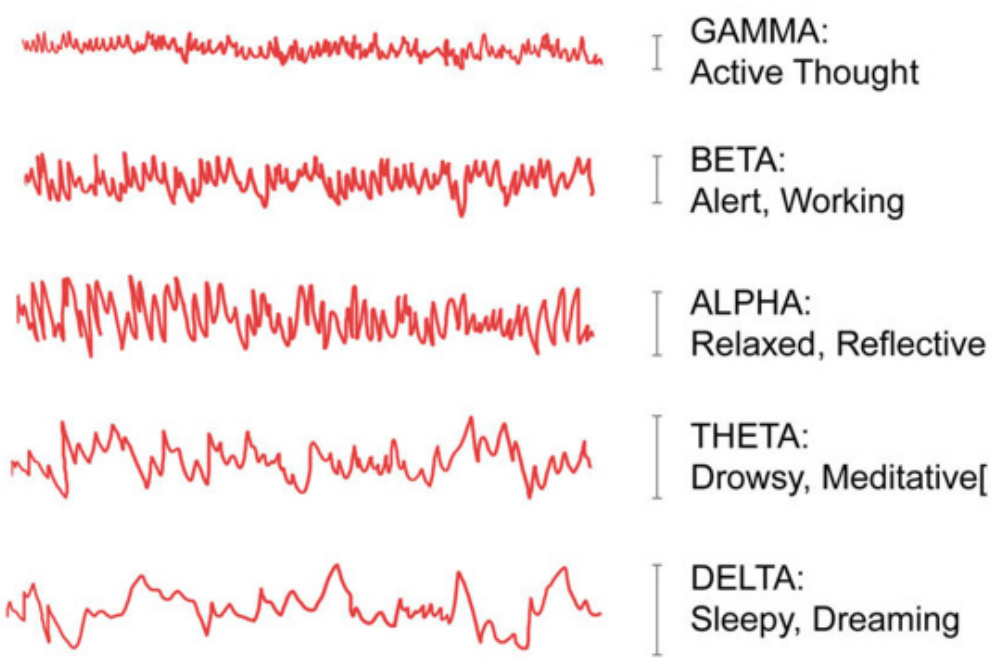

FIGURE 3.3: Spectrum of brain waves from high frequency (Gamma) to low frequency (Delta) [6]

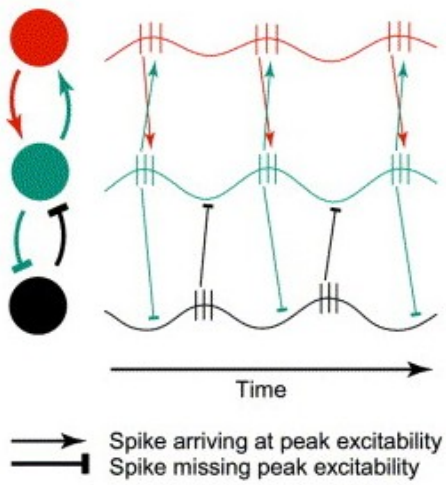

FIGURE 3.4: Communication between neuronal populations through phase synchronization. Spikes that arrive at excitability periods of the receiving neuronal group have pointed arrowheads. Spikes that miss excitability periods have blunt arrowheads. The red and green neuronal groups undergo coherent excitability fluctuations and their communication is therefore effective. The black neuronal group however undergoes excitability fluctuations that are not coherent with the green neuronal group and therefore communication between the green and the black neuronal group is prohibited [7].

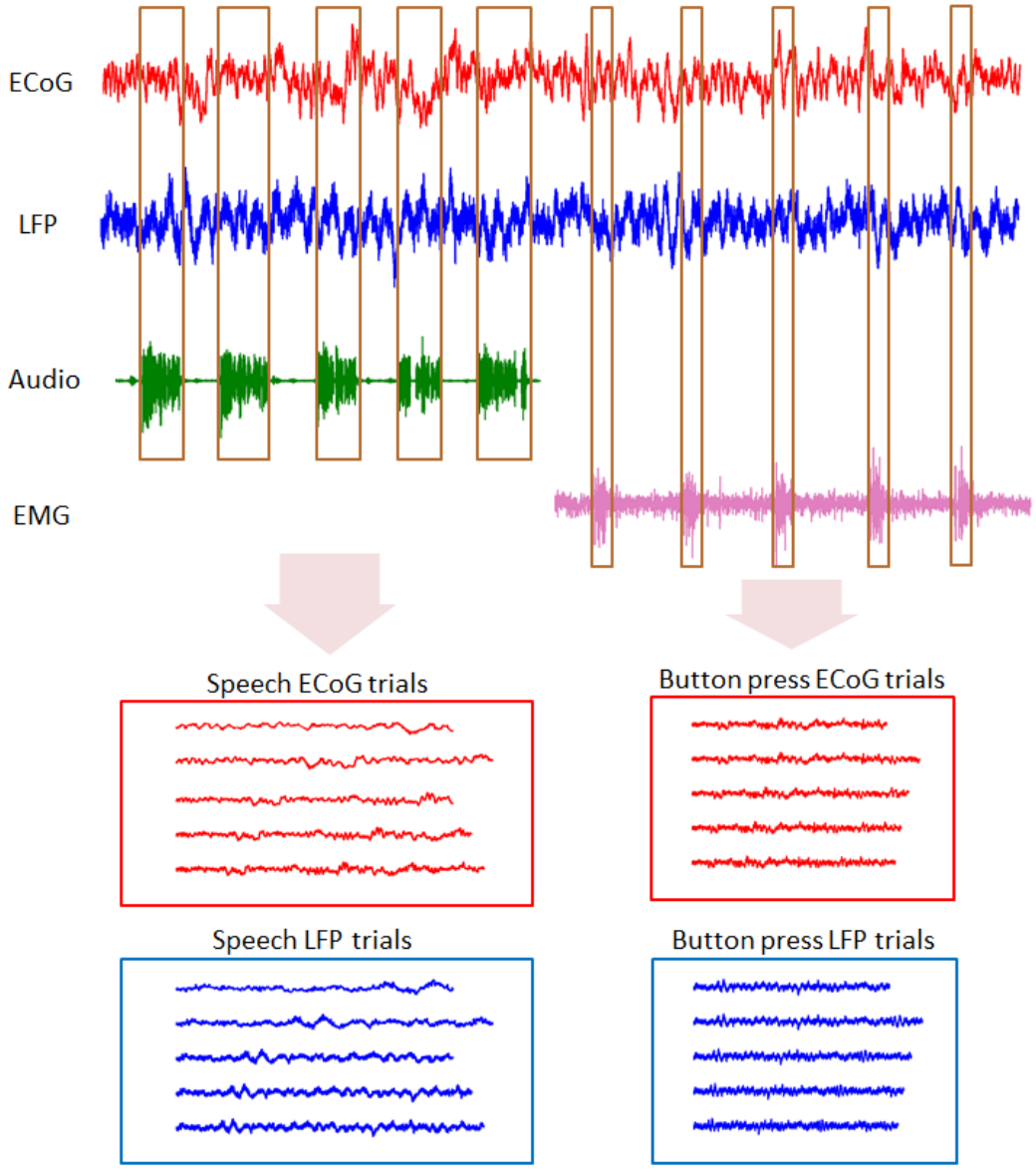

FIGURE 3.5: Segments of data for each trial were extracted based on the recorded Audio or EMG for speech and finger movement tasks respectively.

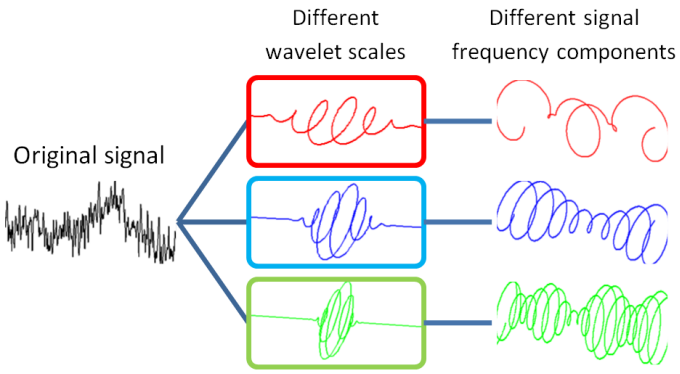

FIGURE 3.6: Complex wavelet transform uses complex wavelets with different scales to decompose the signal into different frequency components.

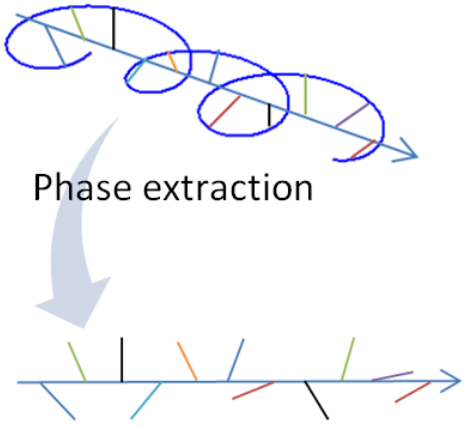

FIGURE 3.7: For each data point, the phase of the complex value is obtained to form a sequence of phases.

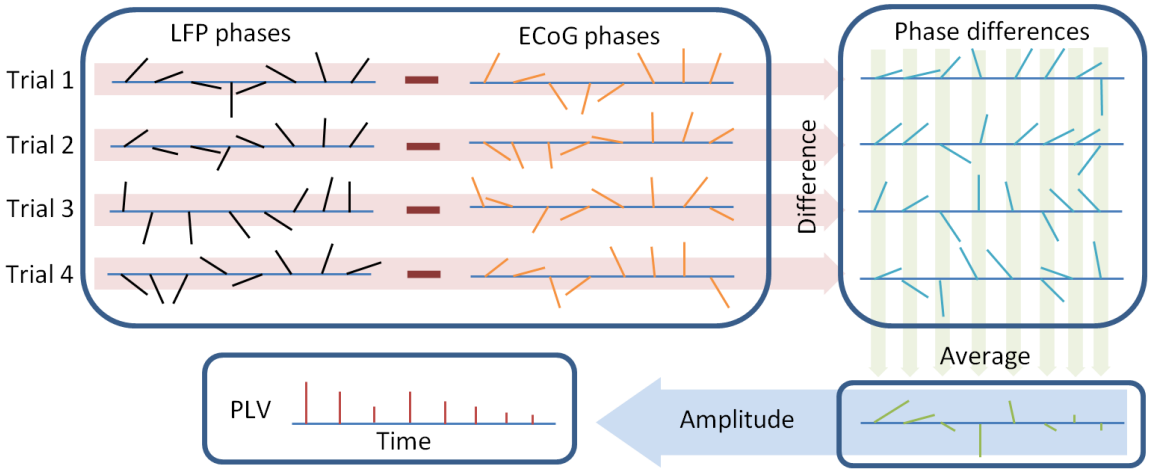

FIGURE 3.8: Procedure of calculating phase locking values. The phase difference between two channels (STN LFP and PFC ECoG) are calculated. Phase differences are averaged over trials and their absolute values are calculated as the plv of the channels.

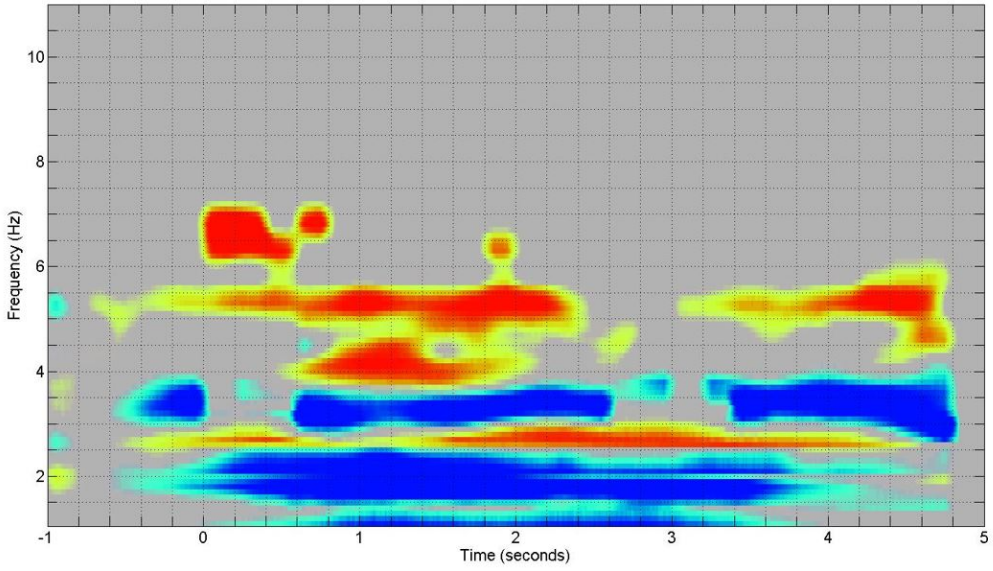

FIGURE 3.9: PLVs are segmented into time-frequency windows of size 0.5 Hz by 200 ms.

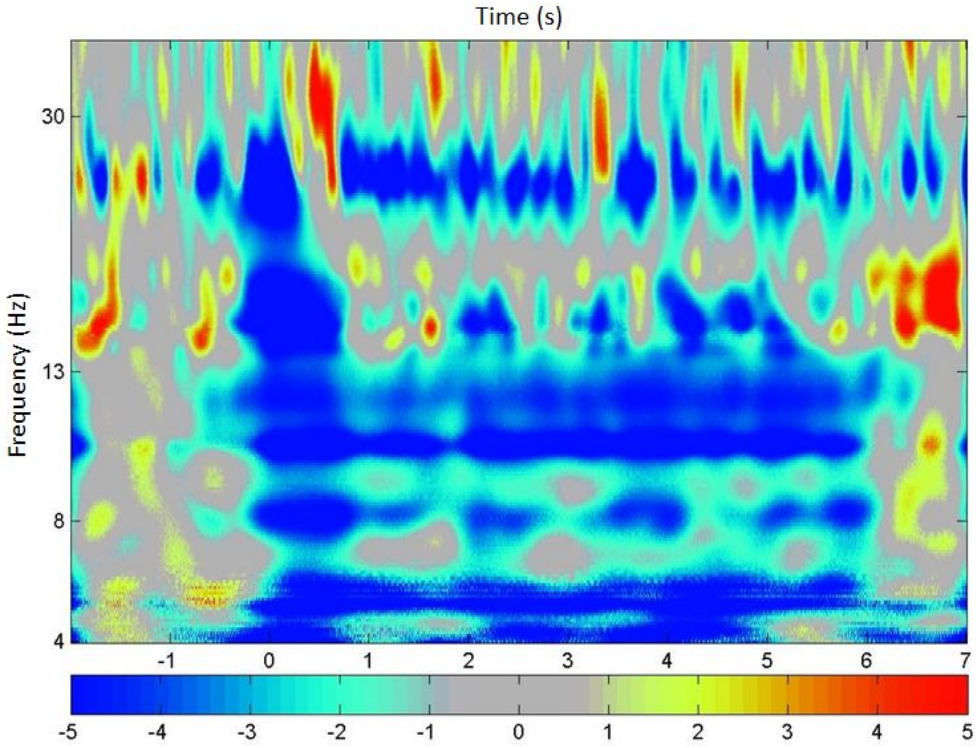

FIGURE 3.10: Spectral power corresponding to alpha and beta range for subject 5 are suppressed around 500 ms before the speech task onset (0s) and lasts until the task offset (6s).

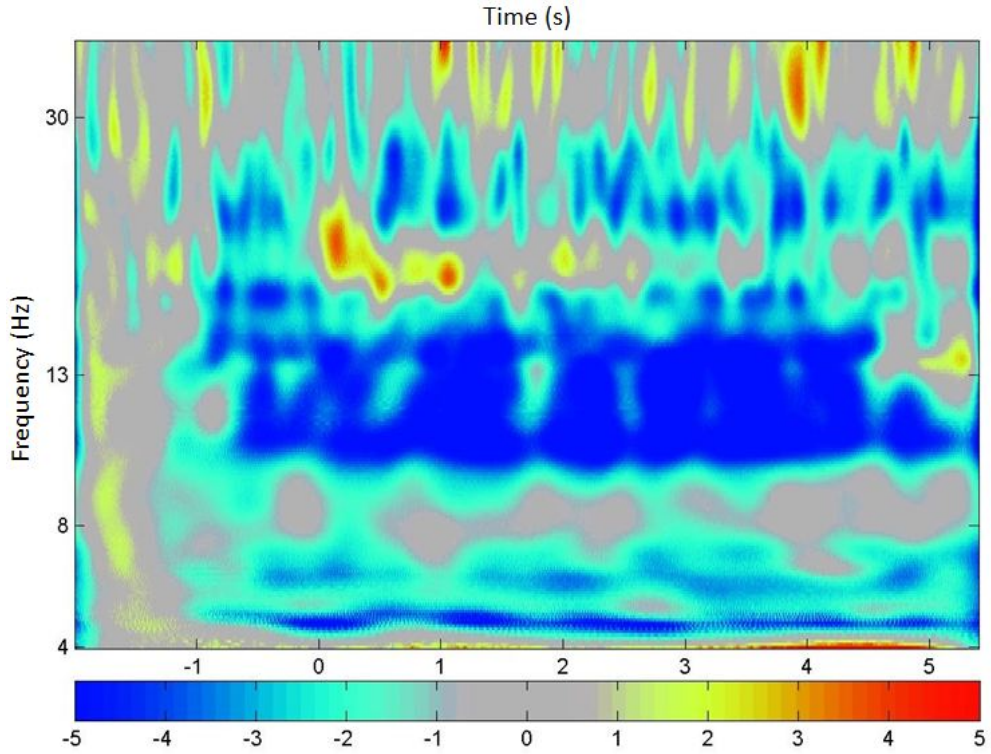

FIGURE 3.11: Spectral power corresponding to high alpha and low beta range for subject 1 are suppressed around 500 ms before the speech task onset (0s) and lasts until the task offset (6s).

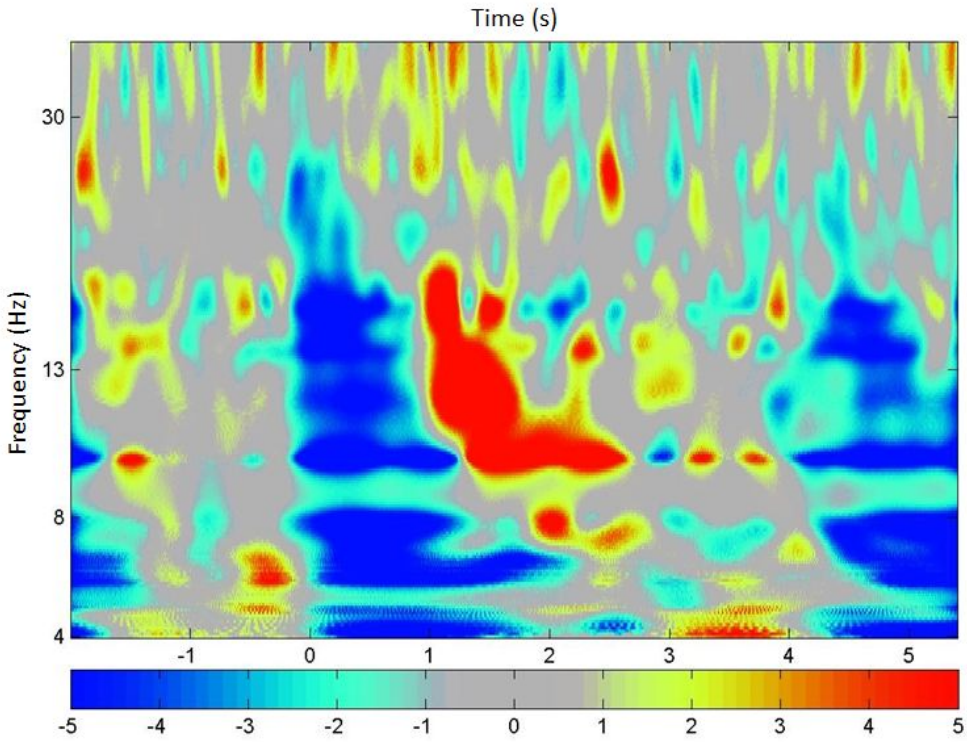

FIGURE 3.12: Spectral power corresponding to theta, alpha and beta range for subject 5 are suppressed around 500 ms before the speech task onset (0s) and is followed by a significant augmentation 1s after onset.

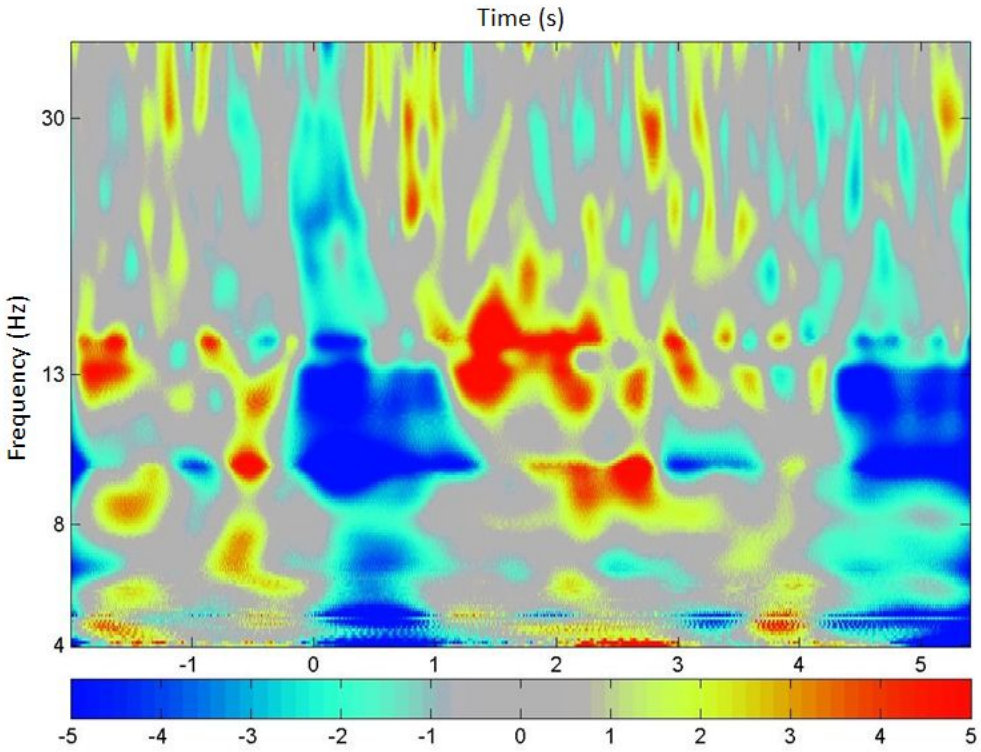

FIGURE 3.13: Spectral power corresponding to alpha and low beta range for subject 1 are suppressed around 500 ms before the speech task onset (0s) and is followed by a significant augmentation 1s after onset.

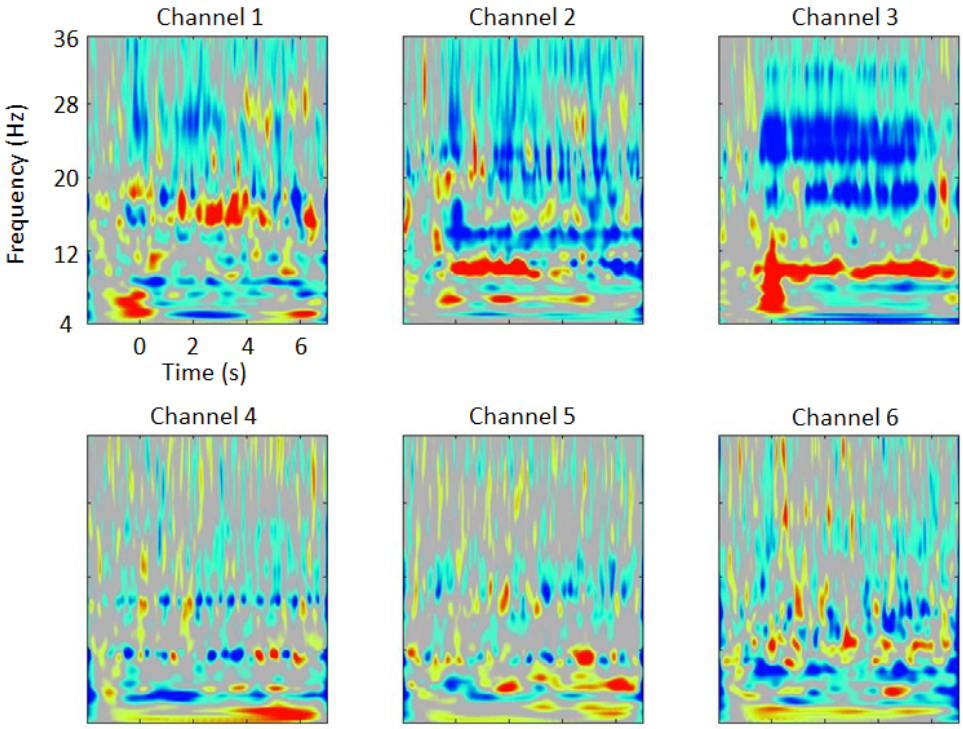

FIGURE 3.14: Described task modulated pattern for speech in subject 3 is significant in channel 3 while channels 4-6 demonstrate random task independent fluctuations.

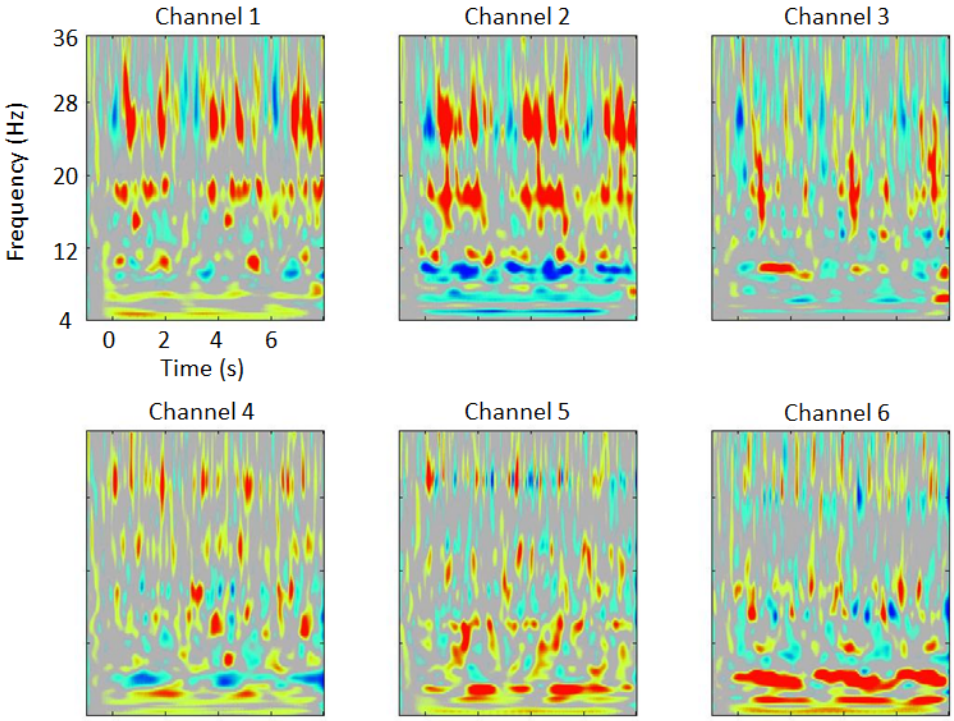

FIGURE 3.15: Described task modulated pattern for finger movement in subject 3 is significant in channel 2 while channels 4 and 5 demonstrate random task independent fluctuations.

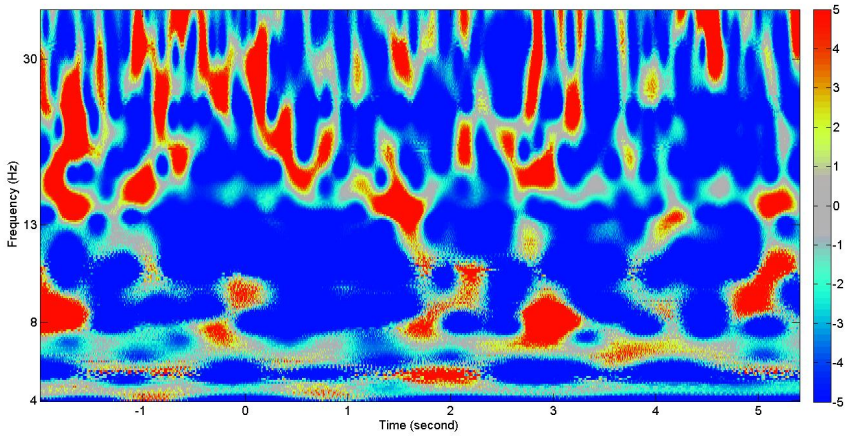

FIGURE 3.16: Single trial spectral power corresponding to alpha and beta range for subject 1 for speech trial.

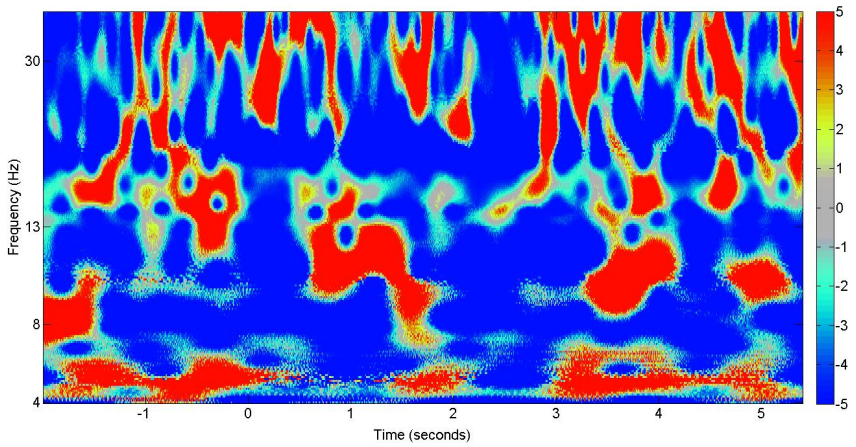

FIGURE 3.17: Single trial spectral power corresponding to alpha and low beta range for subject 1 for finger movement trial.

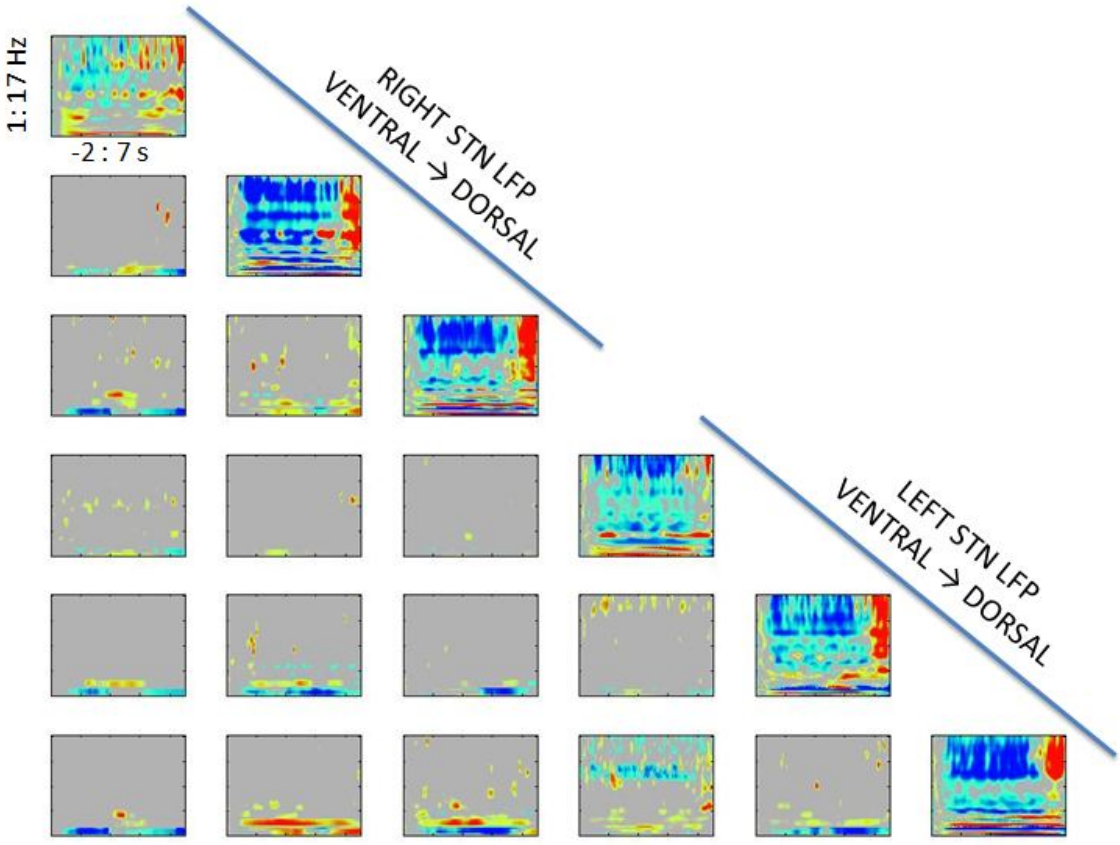

FIGURE 3.18: Spectrograms of PLVs across 6 LFP channels implanted in right and left STN for speech task. In the spectrogram resulting from the connectivity of second right channel and third left channel a significant synchronization can be observed around 4 Hz during the speech task.

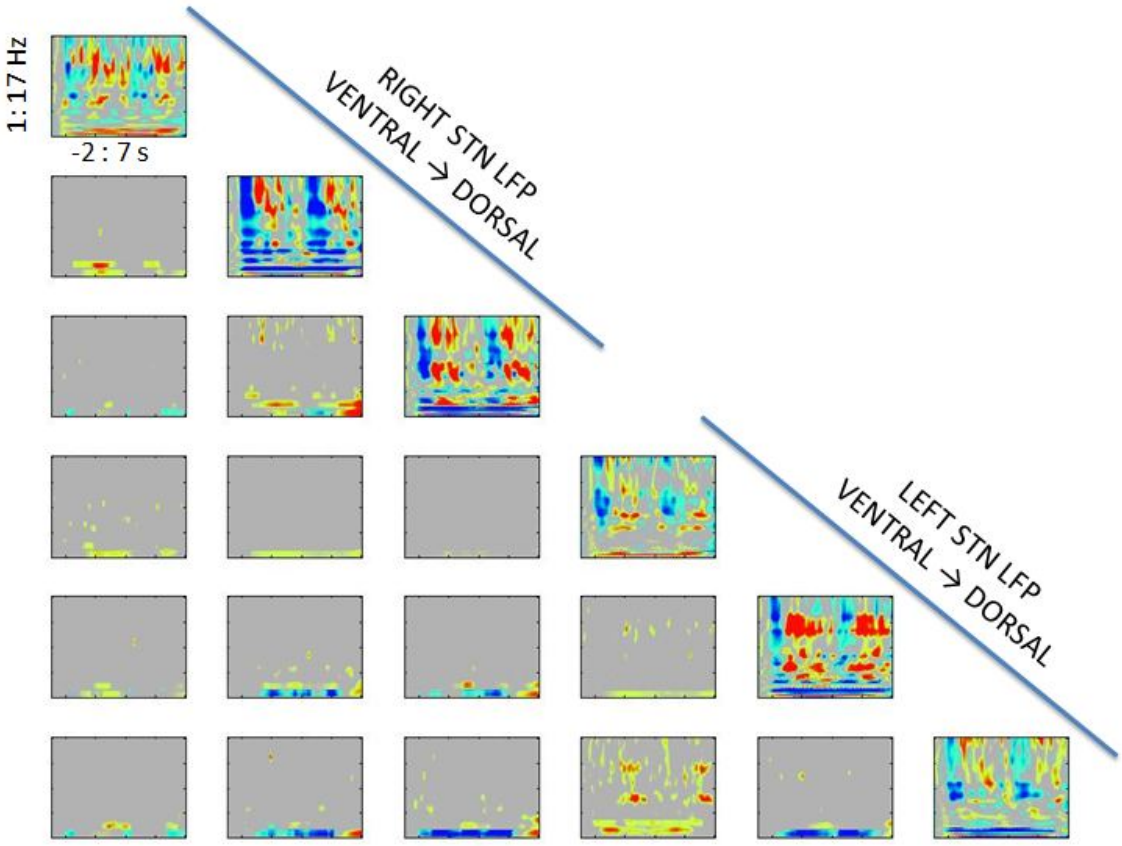

FIGURE 3.19: Spectrograms of PLVs across 6 LFP channels implanted in right and left STN for motor task. In the spectrogram resulting from the connectivity of third right and second left channels as well as third right and third left channels, significant synchronizations can be observed around 4 Hz during the motor task.

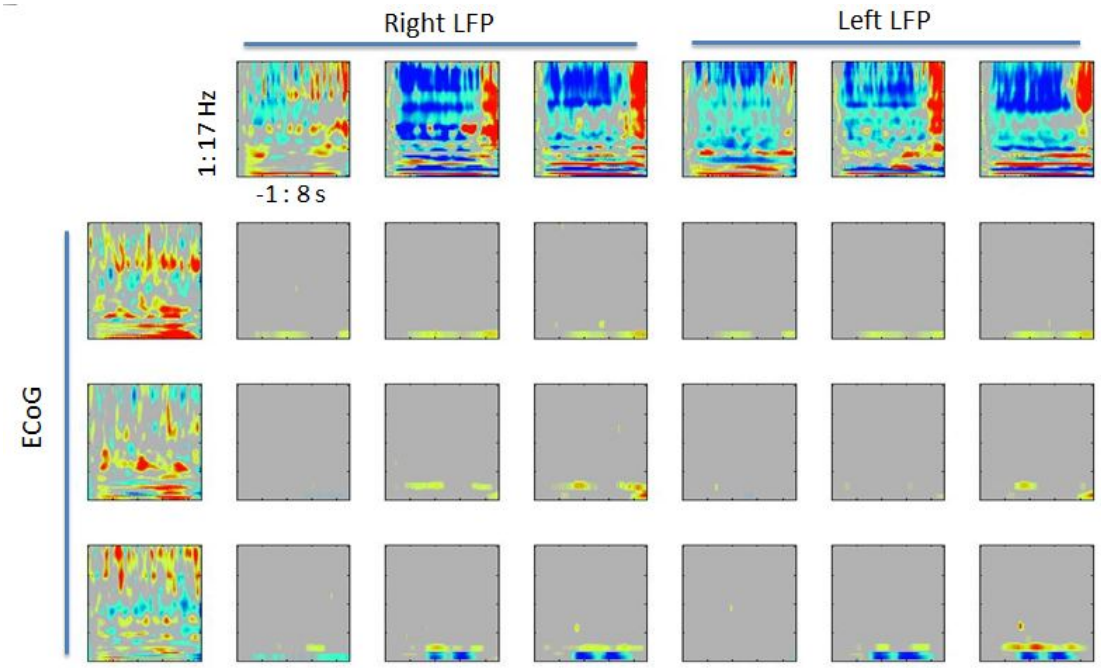

FIGURE 3.20: Spectrograms of PLVs across 6 LFP channels Vs. 3 ECoG channels implanted in right and left STN as well as PFC for speech task. In the spectrogram resulting from the connectivity of third right LFP channel and second ECoG channel, a significant synchronization can be observed around 4 Hz during the speech task.

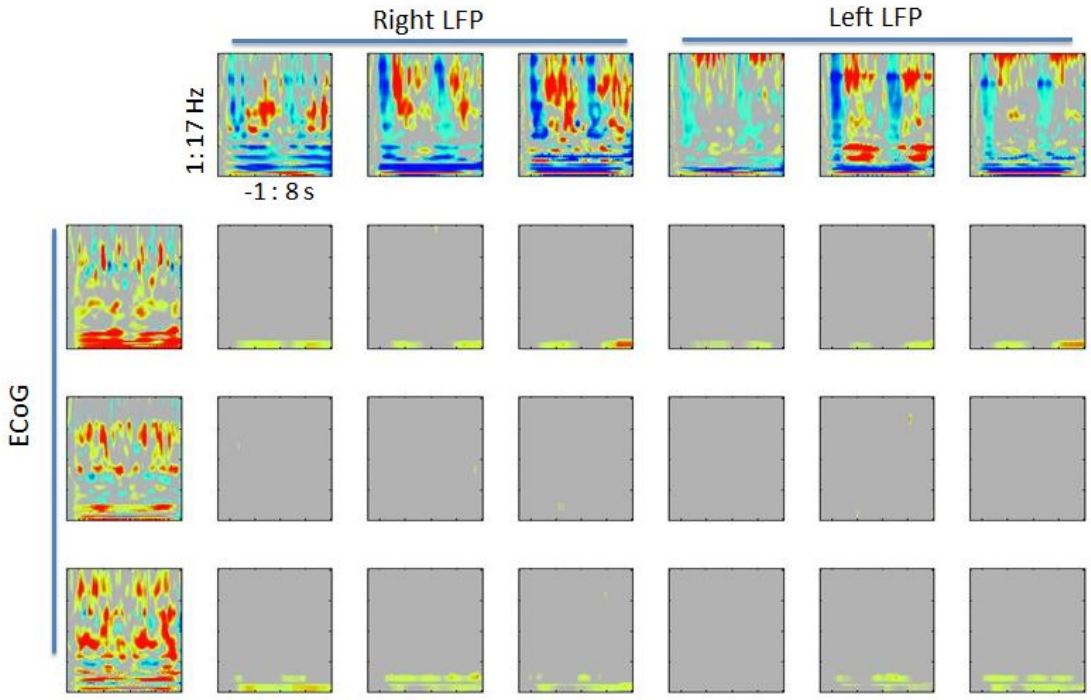

FIGURE 3.21: Spectrograms of PLVs across 6 LFP channels Vs. 3 ECoG channels implanted in right and left STN as well as PFC for speech task. In the spectrogram resulting from the connectivity of third right LFP channel and second ECoG channel, a significant synchronization can be observed around 4 Hz during the speech task.

Chapter 4

Classification of Behavioral Tasks

A system for recognition of patient's activities by analyzing the LFP brain signals is introduced. We only use the data recorded at University of Washington. Wavelet coefficients are the features that describe the LFP signal and support vector machine (SVM) is the classifier that predicts the patient's task.

4.1 Background

The electrical potential recorded from the implanted DBS electrodes may provide substantial information related to subject behavioral goals, and therefore is a candidate signal for an adaptive or closed loop DBS system. Further, electrical potentials recorded from the cerebral cortex have successfully been used in brain-computer interface tasks. This chapter aims at exploring the subcortical electrical potentials in the human brain, obtained during surgical implantation of a DBS system and classification of three different tasks (speech, motor and random) as a part of designing a closed loop DBS system.

LFP recordings, which represent coherent activity of small cell assemblies, have been used in humans to characterize activity within cortical regions and subcortical nuclei [49].

As illustrated in Chapter 4, Time-frequency analysis of motor cortex ECoG [50] and subthalamic nucleus (STN) LFPs [51], has revealed characteristic suppression of beta (13-30Hz) band and augmentation of gamma (30-70Hz) band power preceding and during motor behaviors. Thus, the human subthalamic nucleus in PD exhibits oscillatory behavior in a broad frequency band is modulated by motor activity.

4.2 Classification Method

The procedure of decoding the LFP signals into behavioral tasks includes three phases: (1) preprocessing, (2) feature extraction, and (3) classification.

4.2.1 Preprocessing

LFP recordings are bipolar re-referenced by subtracting adjacent contacts (1-0, 2-1, 3-2). Hence the power line interference (PLI) is removed without any filtering related distortions. An FIR zero-phase filter with transient band of 40-50Hz is applied on data using the `filtfilt` function implemented in Matlab [46]. After applying the anti-aliasing filter, the signals are downsampled to 100Hz. Segments of data with 3 seconds duration, starting from 0.5 second before the trial onsets are extracted as the samples.

4.2.2 Feature Extraction

Features are certain characteristics of the data that are significantly useful for distinguishing different classes. In this technique, features are the time-frequency components of the LFP segments.

Based on the findings of Chapter 3, the task related patterns in LFP data fall into the alpha and beta range (8-30 Hz). Therefore wavelet transform of the data segments

corresponding to this range is calculated. Complex Morlet wavelet is used for transformation and the absolute value if the results is then used as the features.

Due to the high dimensionality of the features, Principal Component Analysis (PCA) is used to reduce the number of features from 9200 to 47 for each sample [52]. In the PCA analysis, each sample is a trial with 9200 features which are the number of time frequency values associated with that trial.

PCA finds the linear combination of features that have the most variance across trials. Therefore the time-frequency points are linearly combined and the top 47 of them that has the most variance are selected. For example, for a subject with task related patterns in the frequency range of 8-15 Hz, these selected components are most likely the linear combination of points corresponding to this frequency while for a subject with task related patterns in 15-30 Hz, the higher frequency points have higher weights in the selected components.

4.2.3 Classifier

Classification is the process of determining that the input data is closest to which predefined class. In this dissertation, the input data are the time-frequency features extracted from data segments and the predefined classes are speech, finger movement or rest.

Support Vector Machine (SVM) is a state-of-the-art method for classification and regression which was introduced by Cortez and Vapnik [53]. It has been used widely in pattern recognition and brain computer interfaces [54]. SVM finds an optimal hyperplane that separates the two training classes. As seen in Figure 4.1 the samples of a class located in the closest distance of the other class are called support vectors and the margin is the distance between the hyperplane and the support vectors. SVM orients the margin in a way that it is maximized.

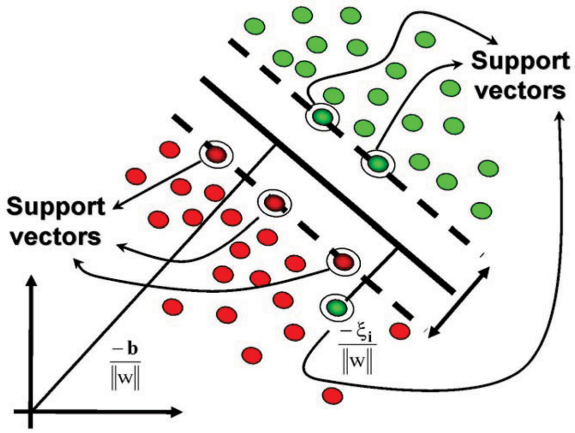

FIGURE 4.1: SVM uses risk optimization to compare various separating hyperplanes and chooses the model with the largest margin of separation [8].

Given (x_i, y_i), $i = 1, 2, \ldots, N$ as N training set of samples where $x_i \in R^d, y_i \in \{-1, +1\}$, SVM solves the following optimization problem described in [**?**]:

$$\begin{aligned} \text{Minimize} \quad & \frac{1}{2}\mathbf{w}^t\mathbf{w} + C\sum_{i=1}^{N}\xi_i \\ \text{Subject to} \quad & y_i(\mathbf{w}^t\phi(x_i) + w_0) \geq 1 - \xi_i, \quad \xi_i \geq 0 \end{aligned} \tag{4.1}$$

The function $\phi(.)$ maps the vectors x_i into another space so that $\phi(x_i)$'s are linearly separable. $C \geq 0$ is the penalty parameter of the error term. Lagrangian method is used to solve the optimization problem. One maximizes the dual variable lagrangian:

$$\begin{aligned} \text{Maximize} \quad & \sum_{i=1}^{N}\lambda_i - \frac{1}{2}\sum_{i,j}\lambda_i\lambda_j y_i y_j \mathbf{x_i}^t\mathbf{x_j} \\ \text{Subject to} \quad & 0 \leq \lambda_i \leq C, \quad \sum_{i=1}^{N}\lambda_i y_i = 0 \end{aligned} \tag{4.2}$$

A kernel function is defined as $K(\mathbf{x_i}, \mathbf{x_j}) = \phi(\mathbf{x_i})^t\phi(\mathbf{x_i})$. The Radial Basis Function (RBF) is given as $K(\mathbf{x_i}, \mathbf{x_j}) = \exp\gamma\|\mathbf{x_i} - \mathbf{x_j}\|^2$.

A proper parameter setting improves SVM classification accuracy. There are two parameters to be set in the SVM model with RBF kernel: C and γ. Instinctively the

γ parameter defines the distance a single training example can reach, which low values correspond to far distances and vice versa. The C parameter trades off training examples misclassification against decision surface simplicity. A low C ensures a smooth decision surface while a high C attempts to classify training examples correctly. Experiments are undertaken to evaluate SVM performance through variations of the C and γ parameters.

KNN is a type of classifier that makes decision based on the classes of k nearest training data [55]. In this dissertation the distance between the two data points is calculated using the l2-norm.

4.3 Experimental results

As described in the previous section, the signal is downsampled to 100 Hz to reduce the computational complexity. Downsampling did not have a significant negative effect on the classifier performance.

4.3.1 Feature Extraction

Wavelet coefficients corresponding to the frequencies between 8 Hz and 30 Hz with the frequency interval of 1 Hz and a time window from 500 ms before onset to 3500 ms after onset were used as features for motor and speech task samples. For the random segments, a time window with the same size is applied to the random parts of signal. Note that the time frequency representation of a random segment can be any randomly shifted rectangle in Figure 4.2 along the time axis.

4.3.2 Classification

LibSVM toolbox is used for classification [56]. Empirically (using the evaluation data) C and γ parameters are set to be 500 and 1, respectively. Three binary classifiers are

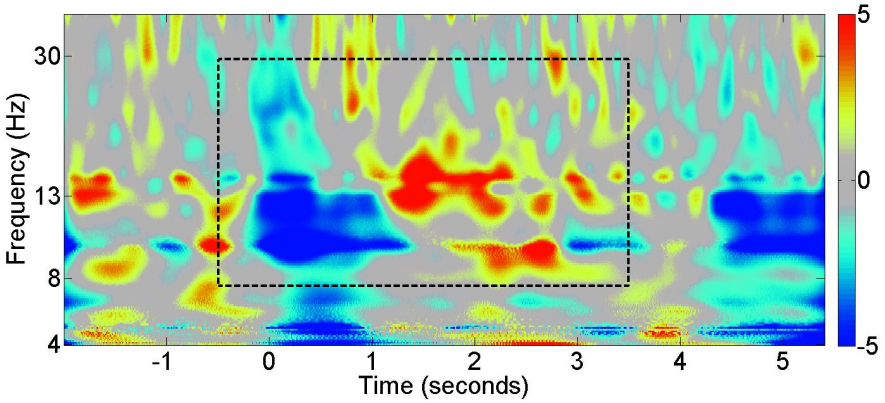

FIGURE 4.2: Time-frequency window selected for extracting the features. Each window starts from half a second before onset and lasts for 4 seconds.and contains freqiency components corresponding to 8-30 Hz.

used for different permutations of tasks (i.e. motor Vs. speech, motor Vs. random, and speech Vs. random). Also a trinary classification was done for all the tasks.

The results of the SVM classifier is compared with the k-nearest neighbor (KNN) classifier [55] with three different k values($k = 1, 3, 5$) and Euclidean distance. In both methods, the principal component analysis (PCA) [52] was performed before classification for reducing the dimensionality of data from 9200 to 47 features. For the evaluation of the classifiers, 10-fold cross validation method is used and the results are presented in Table 4.1.

TABLE 4.1: Averaged percentage of classification accuracies for SVM and KNN classifiers

	SVM		KNN		
	linear	RBF	k=1	k=3	k=5
speech Vs. motor	**81.44**	81.36	66.20	66.42	66.90
speech Vs. random	**81.69**	76.56	76.72	69.46	67.35
motor Vs. random	**84.08**	82.03	76.93	74.89	73.26
all three classes	**73.24**	66.50	62.69	58.75	57.23

Two different kernel functions have been used for SVM classification: RBF and linear. The linear function is claculated by the inner product of two vectors: $k(\mathbf{x}, \mathbf{y}) = \mathbf{x}^t\mathbf{y} + c$ where c is an optional constant. Figure 4.3 presents the comparison results.

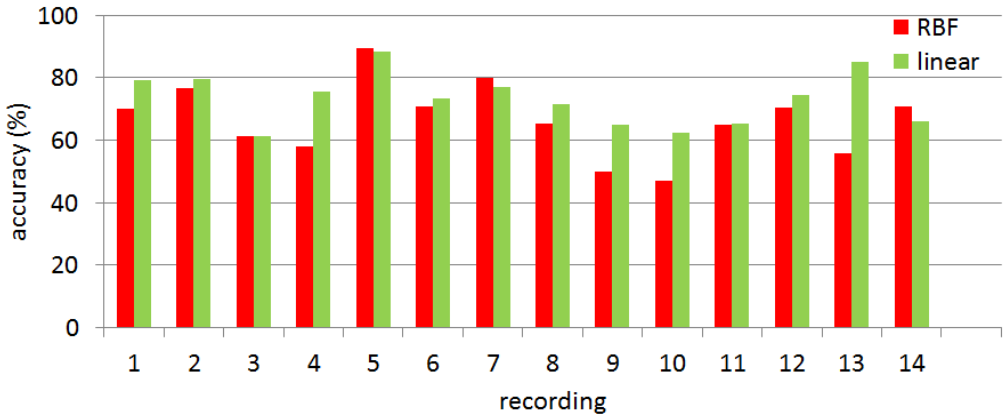

FIGURE 4.3: Three class classification results for linear and RBF kernel SVM.

4.4 Discussion

Table 4.1 shows that SVM outperforms KNN in task recognition experiments. For KNN, as the dimensionality increases, the distant to the nearest data point approaches to the distance to the furthest data point. Therefore, the high number of features causes the decrease in the performance of the KNN method [57]. Also due to the high dimensionality of features, linear kernel function provides a more proper mapping rather than RBF [58].

The variety of behavioral tasks in this research was limited by the restricted time in the operating room to perform the tasks. The reason behind using random segments for classification is to train the classifier to distinguish "other tasks" rather than speech and motor. The classification results for different pairs of tasks (rows 1 to 3 in Figure 4.1) show that the classifiers performances for speech Vs. motor is nearly the same when one is random. This verifies that random segments are proper representations for "other tasks".

Figure 4.3 demonstrates that some recordings lead to a highly accurate classification (recording 5) while for some others the results are relatively poor (recordings 3, 9, and 10). Even for different recordings of the same subject (recordings 8 and 9 from subject 6) classification accuracy is considerably different (see Table 2.2 for information about the

recordings). This may be due to the variations in positioning the recording electrodes.

The classification results show that the SVM classier is more accurate in distinguishing all the tasks rather than the KNN. Also linear kernel function provides a better mapping for the SVM rather than the RBF function and can be considered as a proper tool for task recognition for a closed loop DBS system.

The proposed classification technique can be utilized as the initial step of designing a high level DBS system. Recognizing patient's current task can be led to an optimal DBS parameter adjustment to decrease the side effects.

Chapter 5

Asynchronous Detection of Movement

This chapter introduces an event detection method based on STN LFP data. The LFP data is recorded bilaterally from patients with PD during button pressing tasks. Inter-hemispheric connectivity of STN between every bilateral pair of channels is measured as a 1-D time series signal and using the PCA, the most distinguishing component is selected. Fig.5.1 illustrates a brief overview of the event detection procedure by which the bilateral recordings are translated to events and nonevents time series.

5.1 Background

Most daily activities are self-paced meaning that the patient spontaneously initiates the activity on her/himself without receiving any external cues. Thus an "asynchronous" behavior detector is required to classify the neural data into active or idle classes. Electroencephalogram (EEG) based systems has been widely used in such cases. Temporal modeling

of EEG during self-paced hand movement is investigated and used in unsupervised movement onset detection [59, 60]. Event-related (de)synchronization (ERD/ERS) is used to detect the neural correlates of self-paced motor activity [61]. Furthermore onset detection is applied for detecting various movement intentions: reaching [62], cursor control [63], task force and speed [64] and movement directions [65]. Electrocorticographic (ECoG) signals has also been a popular source for activity detection. The ERD/ERS movement related patterns in single-channel ECoG is investigated [66] and onset and direction of movements are decoded using human ECoG [67]. In [68] they developed a method for grasp detection from Human ECoG during natural reach-to-grasp movements. Temporal alignment of ECoG recordings for upper limb movement is measured and used for activity detection [69]. Intracortically recorded spiking neural signals are also attractive for movement intention detection because they can in principle provide greater fidelity of encoded information compared to ECoG and EEGs [70]. As another example, the Utah Electrode Array (UAE) was used to detect and classify multiple finger movements [71].

Unlike the EEG and ECoG data, local field potentials (LFP) recorded from the basal ganglia has been rarely used for activity recognition. Mace et al. proposed an automated approach towards detecting complex behaviors [72]. They calculated the detection contours and adaptive thresholds to produce a binary signal indicating the presence (or absence) of an event. LFP recorded from the STN of patients with PD has shown to be modulated by speech production and finger movement [3]. The event related time-frequency patterns during these tasks were used to classify multiple behavioral tasks: speech, motor and rest [73]. This classifier is one step closer to a closed-loop DBS system that uses STN LFP as the feedback source; however it requires a priori knowledge of trial onsets which enforces a major limitation on the system. A more practical closed-loop DBS system would asynchronously detect patient's behaviors.

STN recordings from the two hemispheres are non-stationary measures meaning that the activity in a given area spreads to other areas over time [74]. This leads to group delay (frequency variant phase delay that leads to a constant time delay and doeas not distort the signal) among sources [75] where measuring their connectivity requires nonlinear methods. Linear methods are based on intercorrelation or coherence functions and do not consider the group delay among sources. On the other hand nonlinear methods such as non-linear regression [76, 77], mutual information [78, 79] or synchronization of phases [43, 80] use various techniques to compensate for the group delay originated from the distance of the sources. In this study, we use the nonlinear regression method to calculate the amount of interdependency among bilateral recordings.

5.2 Detection Method

5.2.1 Preprocessing

LFP recordings of each hemisphere were bipolar re-referenced by subtracting adjacent contacts (1-0, 2-1, 3-2). This way power line interference (PLI) was removed without any filtering related distortions. An FIR zero-phase filter with transient band of 80-100Hz is applied on data using the `filtfilt` function implemented in Matlab [46]. After applying the anti-aliasing filter, the signals were downsampled to 200Hz.

5.2.2 Non-linear Regression

Nonlinear regression of signal X and signal Y was calculated based on an estimation of non-linear correlation $h^2_{XY}(\tau)$ which represents the dependency of the signal Y on the signal X when signal Y is shifted τ samples forward in time:

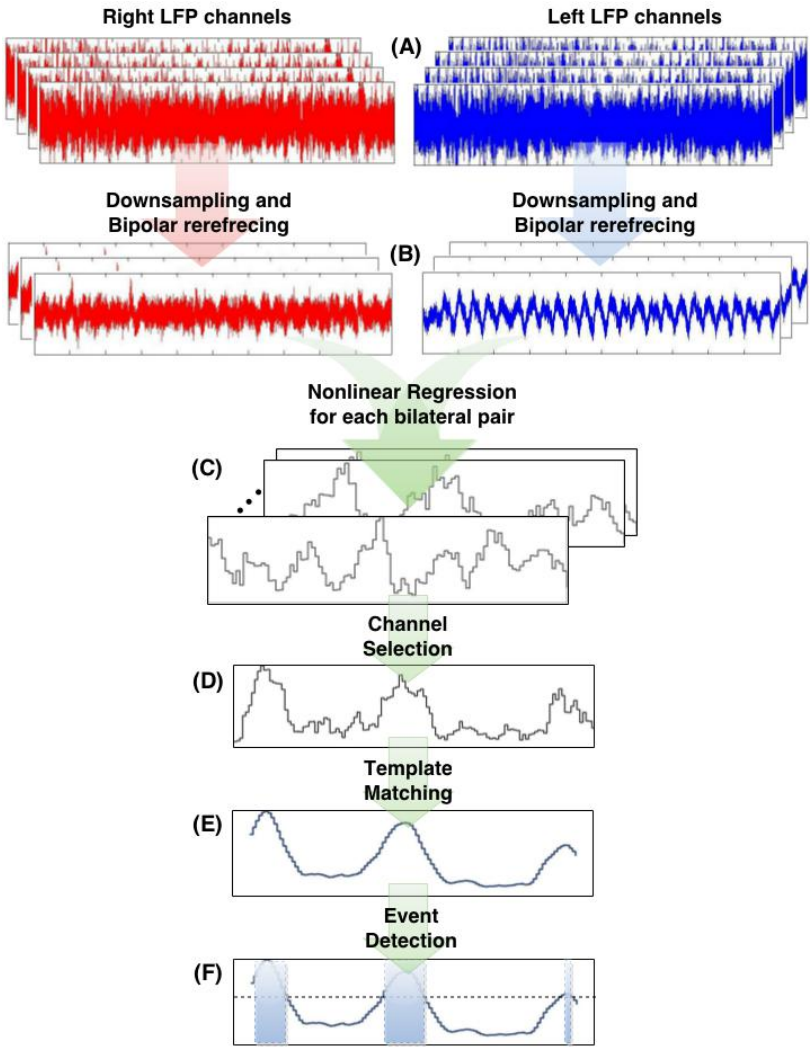

FIGURE 5.1: (a) LFP data are recorded from all four channels of each DBS lead located in each hemisphere. (b) Signals are bipolar re-referenced and downsampled. (c) Intercorrelation between each bilateral pair of channels is measured as $h^{2*}_{XY}[n]$ (total of 9 pairs). (d) A linear combination of channels is selected using PCA. (e) Correlation between $h^{2*}_{XY}[n]$ and the template is calculated to derive the feature vector $\gamma^{2*}_{XY}[n]$. (f) Single events are detected by thresholding the values of $\gamma^{2*}_{XY}[n]$.

$$h^2_{XY}(\tau) = 1 - \frac{VAR(Y[n+\tau]|X[n])}{VAR(Y[n+\tau])} \tag{5.1}$$

where $VAR(Y[n+\tau]|X[n])$ is the conditional variance of $Y[n+\tau]$ given $X[n]$ (see appendix I). The highest amount of non-linear correlation for a limited range of time shifts

is calculated which leads us to non-linear correlation coefficient:

$$h^{2*}_{XY} = max_{\tau}\ h^{2}_{XY}(\tau)$$
$$\tau_{min} \leq \tau \leq \tau_{max} \tag{5.2}$$

To simulate the real time implementation of non-linear regression, rectangular windows of one second are applied to the downsampled data where the overlap of the two consequent windows is 90% of the window length (Fig. 5.2(a,b)). This leads to a time series of correlation coefficients $h^{2*}_{XY}[n]$ with the sampling period of 50 ms (Fig.5.2(c)). To implement the time shifting, the second channel windows shifted with respect to the first channel windows to form $Y[n+\tau]$.

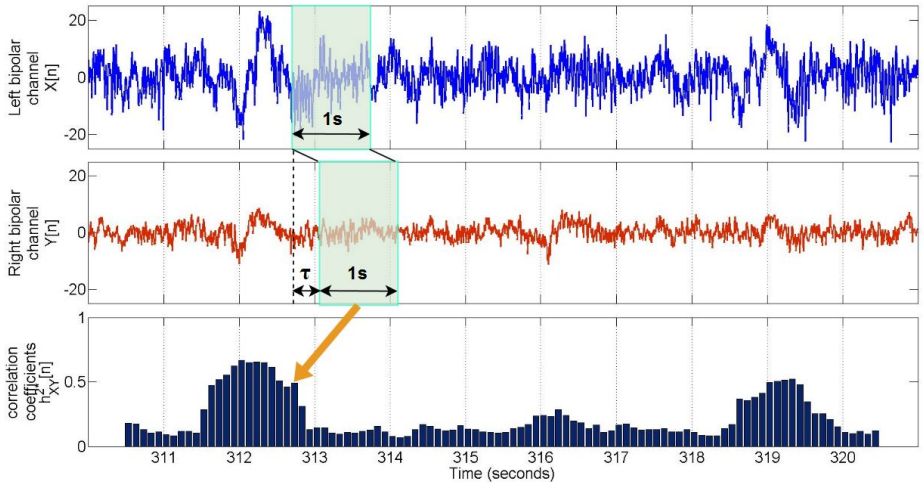

FIGURE 5.2: Time windowing of two channels for non-parametric non-linear regression analysis.

5.2.3 Component Selection

Correlation coefficients $h^{2*}_{X_iY_j}[n]$ corresponding to every possible bilateral pair is calculated where $i, j = 1, ..., N_{ch}$ and N_{ch} is the number of bilateral pair of channels. The optimum component $c^{2*}_{XY}[n]$ is calculated using the optimum component coefficients λ^* obtained from training data using principal component analysis (PCA)(see appendix):

$$c_{XY}^{2*}[n] = \sum_{k=1}^{{N_{ch}}^2} \lambda^* h_{X_i Y_j}^{2*}[n] \tag{5.3}$$

5.2.4 Template Matching

A template matching technique using normalized correlation coefficient is used to find the occurrences of button pressings in the simulated real time data. The technique includes creating the template (training phase) and template matching (testing phase):

5.2.4.1 Creating the Template

Rectangular time windows of 3 seconds $w[n-k]$ starting from 1.5 seconds (15 samples) before trial onset m_i are applied to each trial i in the first task block and the results are synchronized averaged to form a 3 seconds (30 samples) pattern for each subject [81]:

$$p_{XY}^{2*} = \sum_{i=1}^{N_trial} c_{XY}^{2*}[n] w[n-m_i] \tag{5.4}$$

5.2.4.2 Real Time Template Matching

A time series of normalized correlation coefficients $\gamma_{XY}^{2*}[n]$ between the template $p_{XY}^{2*}[n]$ and the most recent 3 seconds segment of the optimal component $c_{XY}^{2*}[n]$ of the real time data was calculated:

$$\gamma_{XY}^{2*} = \frac{\sum_k p_{XY}^{2*}[k] c_{XY}^{2*}[k-n]}{\sum_k p_{XY}^{2*}[k] \sum_k c_{XY}^{2*}[k-n]} \tag{5.5}$$

Time resolution of $\gamma_{XY}^{2*}[n]$ was determined by the amount of windowing step in each template matching calculation which is assigned 50ms to keep the resolution of$c_{XY}^{2*}[n]$. $\gamma_{XY}^{2*}[n]$ is used as the feature vector for event detection.

5.2.5 Determination of Detected Times

The feature vector $\gamma^{2*}_{XY}[n]$ obtained by template matching method in the previous subsection is now fed to an event detection block to determine the detected times. Let θ be a threshold value of the detection algorithm used to classify binary events. $\gamma^{2*}_{XY}[n]$ values that are higher than θ are considered detected events (ones) and the rest are non-events (zeros) which form a time series of zeros and ones, $b^{2*}_{XY}[n]$.

5.2.6 Evaluation

The digital button channel $ev[n]$ is the ground truth. $ev[n]$ is a time series of binary values which has the same time resolution as $b^{2*}_{XY}[n]$ (50ms sampling period). The length for each button pressing trial was set to 500ms (10 samples) which corresponds to the average duration of the pick in h^{2*}_{XY}. For evaluation, each sample was labeled either true positive (TP), false positive (FP), true negative (TN) or false negative (FN) based on Table 5.1. The number of condition positives and condition negatives were determined by the number of ones and zeros in the $ev[n]$ respectively. Then fundamental measures of detection accuracy were obtained: true positive rate (TPR) and false positive rate (FPR) [82]. As a result ROC curves are created based on TPR and FPR values. When ROC curve is used for evaluation, the area under the curve (AUC) determines the performance of the detector. AUC varies between 0 to 1 and it gives a measure of separability between events and nonevents with the area of 1 for perfect separation.

5.3 Experimental Results

LFP data from eight subjects was utilized in this study. In calculating the nonlinear regression of the bilateral channels, the values of τ_min and τ_max were assigned -100ms and +100ms respectively because the estimated correlation delay time between the channels

TABLE 5.1: Confusion matrix

		Condition (as determined by labels ev)	
		negative $ev = 0$	positive $ev = 1$
Test outcome b^{2*}_{XY}	negative $b^{2*}_{XY} = 0$	true negative TN	false negative FN
	positive $b^{2*}_{XY} = 1$	false positive FP	true positive TP
		false positive rate $FPR = \frac{\sum FP}{\sum FP+TN}$	true positive rate $TPR = \frac{\sum TP}{\sum TP+FN}$

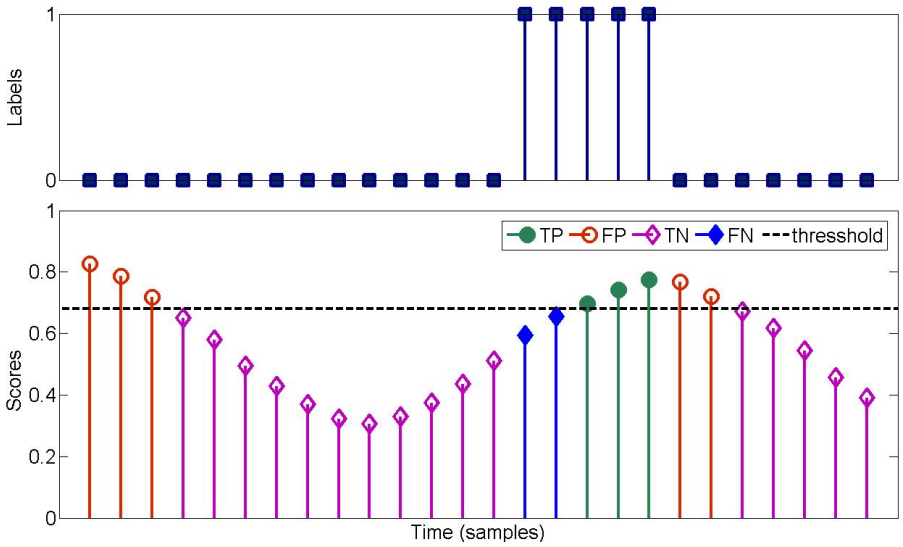

FIGURE 5.3: A segment of labels generated from the digital channel (a) and scores created by the algorithm (b). a threshold of 0.68 is considered for event detection and the samples are labeled as TP, FP, TN, FN based on their score $\gamma^{2*}_{XY}[n]$, threshold θ and the corresponding label sample $ev[n]$.

never exceeded these values during experiments. In a leave-one-block-out technique, for each subject, one trial block was used for creating the template and the remaining trials were used for evaluation. This procedure was repeated until all of the blocks were used exactly once for training. Each ROC curve is interpolated and averaged over iterations to form the subject specific ROC curves in Figure 5.6). Figure 5.4 illustrates the template created from the first trial block for each subject.

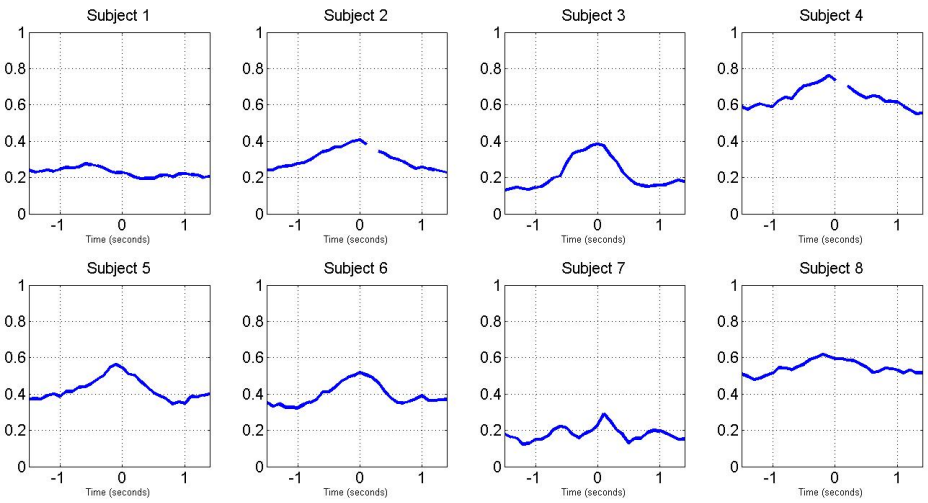

FIGURE 5.4: Templates created from the first trial block for each subject by averaging all the 15 trials. The templates are 3 seconds long starting from 1.5 seconds before the trial onset. The values are normalized and are between 0 and 1.

To investigate the robustness of this method for other behavioral tasks the templates corresponding to speech tasks are calculated and compared the templates corresponding to the finger movement tasks. Figure 5.5 illustrates the templates of the two tasks for the same pair of channels of subject 3. The peak corresponding to the speech tasks is relatively insignificant comparing to the motor task.

To investigate the effectiveness of PCA, we selected the pair of channels resulting in the best results for each subject and ran the algorithm without lection (the dashed line in Figure 5.6).

For a FPR value of 10% the average TPR value is 50% which this increases to 70% and 88% for the accepted FPR values of 30% and 50% respectively. The average AUC for the proposed method without component selection (best pair of channels) is 71% which increases to 78% when component selection is applied. The proposed algorithm demonstrates the highest performance for subjects 2, 3, and 4 where for an accepted FPR value of 50% the TPR is approximately 100%. The lowest results are obtained from subject

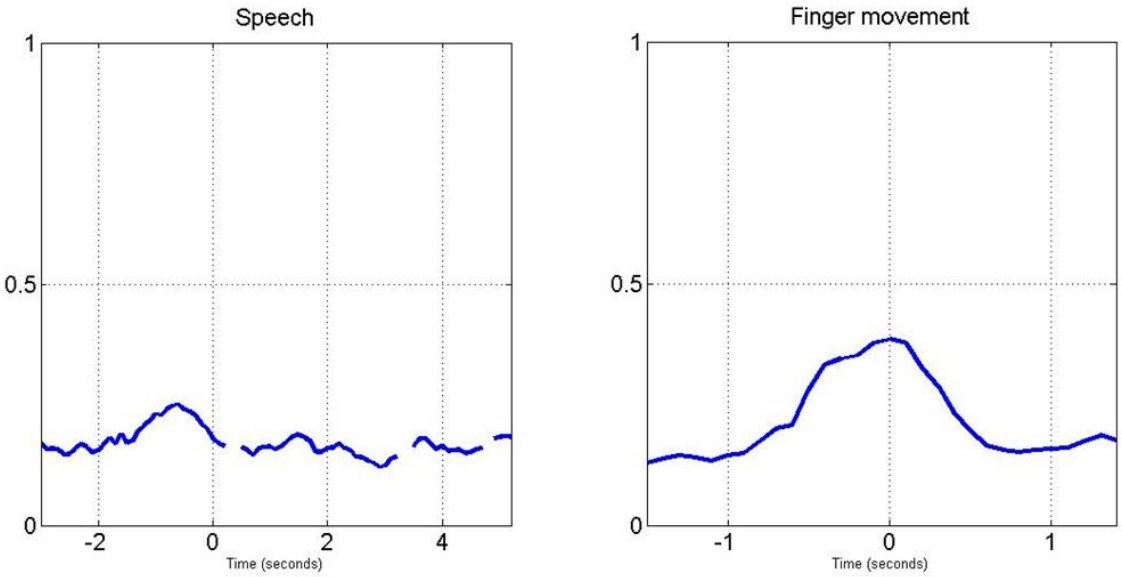

FIGURE 5.5: Templates corresponding to the speech and motor task for subject 3. For motor tasks the templates starts 1.5 seconds before the onset and lasts 3 seconds. For the speech task the template starts 3 seconds before the onset and ends one second after the maximum offset among the trials. The values are normalized and are between 0 and 1. the missing points are Nan values created by division by zero.

8 who was the only subject implanted with the 8 contact electrodes. For this subject the four most frontal contacts of each electrode are used in this study because only these electrodes were targeting the STN. Moreover subject 8 is the only subject that applying the component selection lowered the performance of the algorithm for all the FPR values. On the other hand the component selection represents promising improvement for subjects 1,2,4, and 5.

5.4 Disscussion

Using the proposed detection method, we detected finger movement tasks in patients with PD using nonlinear regression. The only source of information is the LFP signal recorded by the same DBS lead that delivers the stimulation signal. This eliminates the need for wearing additional sensors and eventually diminishes the power consumption.

TABLE 5.2: The values of true positive rate (TPR) for three different false positive rate (FPR) values as well as area under the curve (AUC) for all subjects.

	TPR (%)						AUC (%)	
	FPR = 10%		FPR = 30%		FPR = 50%			
Subject	with PCA	without PCA	with PCA	without PCA	with PCA	without PCA	with PCA	without PCA
1	**38**	12	**62**	37	**88**	56	**74**	56
2	**51**	35	**86**	67	**100**	75	**87**	71
3	69	**77**	88	**95**	**100**	96	90	**92**
4	**52**	44	**84**	65	**99**	83	**85**	75
5	**39**	14	**53**	46	**71**	65	**69**	62
6	20	**40**	58	**66**	**80**	77	71	**74**
7	28	**29**	50	**52**	**83**	67	**71**	63
8	26	**31**	**71**	67	**89**	85	**76**	75

Moreover, an asynchronous detection approach using deep brain LFP may be used in the future implanted BCI systems.

LFP signals were recorded bilaterally from STN and the inter-hemisphere connectivity was measured using nonlinear regression of the sources. In majority of subjects button pressing caused a significant interconnection between the right and left STN. Darvas et al. investigated the motor related bilateral connectivity in STN using phase synchronization [43]. They captured the phase differences between two hemispheres and averaged them over trials. The results showed that button pressing task creates a constant phase difference in a certain frequency range which illustrates the bilateral synchrony of the STN. However the synchronized averaging requires an off-line analysis of the recorded signals which makes it impractical for real-time detection. A nonlinear regression method on the other hand, does not require the statistical analysis of the signal over a long period of time and uses nonlinear matching techniques to measure the connectivity in the real time.

As illustrated in Figure 5.6, subjects undergoing the same experimental procedure produced varying results with different levels of performance. This may be the result of varying electrode placement that is performed based on subjects' responses to simple joint

movements performed by a specialist in the operation room. In a close-loop DBS system, the algorithm can be applied during the surgical procedure to automatically find the optimum depth for the DBS leads using the ROC curves produced by the training data. Also comparing the Figures 5.4 and 5.6 shows that generally the subjects with sharper peaks in the template resulted in the better detection performances.

In this technique, each sample is labeled either as event or nonevent and therefore each button press trial may contain several detected events. Conversely, there are many nonevents labeled between activities. An alternative to this sample-by-sample labeling method is an event-by-event approach where each trial is considered as just one event. Although the event-by-event approach is popular in Brain Computer Interface systems, the sample-by-sample method has provided more promising results in our work. This method seems to be superior for future closed-loop DBS applications where motor events are of arbitrary duration, and detected events will influence time variant DBS parameters.

Low Signal to Noise Ratio (SNR) in single trial classification, unknown trial onset in asynchronous detection, and noisy nature of deep brain LFP data are all serious limitations in designing an accurate detection system. An ideal closed-loop DBS system would detect the daily tasks that are self driven. Hence detection of un-cued events becomes essential in designing such systems. In our previous work we introduced a classification technique that used the pre-determined segments of LFP data to recognize the patient behavior [73].

The template for speech tasks were calculated and investigated in Figure 5.5. However the significance of the peak in the template was relatively poor which led to the poor detection results. As a future work, we can develop a more robust connectivity measurement technique to detect presence of a higher variety of behaviors and by combing it with the classification method we will be able to recognize patients' different behaviors and design a behavioral level closed-loop DBS system.

The algorithm is senstive to the duration of the template. For templates shorter than 3 seconds the output of template matching is noisy with multiple picks for an event thus the FPR rate increases. On the other hand, if the template length increases there will not be any significant change in the performance however the delay of the system increases and in practice, the system detects the behavior when it is already done. Also regarding the extension of the algorithm for detection of multiple behaviors, we must note that the template might be sensitive to the target behavior. For example the template for the speech task would be longer than the template for the button pressing. As a solution, we can use different templates corresponding to different tasks and compare the final results to achieve the output.

Since the closed loop parameter adjustment has not been well defined yet, it is difficult to determine the optimum working point on the ROC curves and eventually evaluate the overall performance of the detector. To determine the working point, it is important to evaluate the risk of any false action. For instance, stimulating with a very high amplitude might cause muscle contraction which might cause a fatal damage to the patients during driving. On the other hand if a certain level amplitude augmentation does not cause any side effects but increase the therapy dramatically, the working point can be selected on the right top side of the curve where we allow a high FPR.

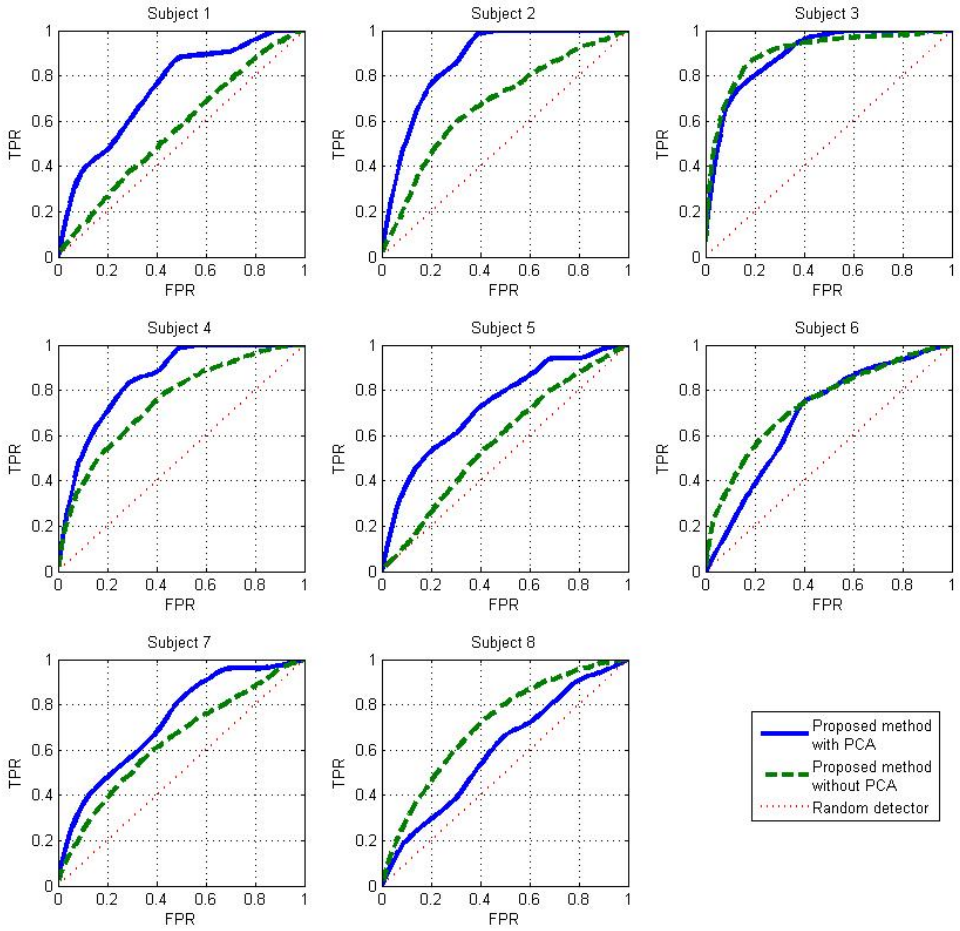

FIGURE 5.6: ROC curves generated for eight subjects. x axis corresponds to the false positive rate (FPR) and y axis corresponds to the true positive rate (TPR) as explained in Section 5.2.6. The ROC curves generated in a leave-one-block-out technique are interpolated and averaged over the iterations to produce these results. The solid line demonstrates the proposed detector performance where any point on the line can be achieved by a certain threshold. The dashed line curve represents the performance of the same technique; but instead of component selection a pre-determined pair of bilateral channels that produced the highest performance is selected. The diagonal dotted line represents the performance of a random detector where every sample is either assigned event or nonevent by a uniform binary random function.

Chapter 6

Conclusion, Discussion, and Future Research Direction

6.1 Conclusion

In this thesis we addressed the important research question of how human behaviotal tasks can be detected and recognized through LFP signals with the implication of designing a behavioral level closed-loop DBS system. We recorded LFP and ECoG from patients with PD during different behavioral tasks and analyzed the data to come up with meaningful features required for task recognition.

A beta and alpha power suppression during speech and a beta and alpha suppression followed by an augmentation in LFP during motor task was observed in majority of subjects. As a result, we used the time frequency features of LFP signal corresponding to beta and alpha range (8-30 Hz) to classify the behaviors. We used a SVM classifier to find the optimum hyper planes that separate the three classes: speech, finger movement, and rest. The performance of SVM was evaluated for different kernel functions and compared to the KNN algorithm. As a result, the SVM with RBF kernel was shown to have the highest

performance which is able to perform binary classification with an average accuracy of 82.40% and 73.24% for three class classification.

Simultaneous recordings of bilateral STN LFP and PFC ECoG provided a great chance for investigating task modulated connectivity in these regions. Using phase synchronization we discovered that there is a task modulated connectivity between the STN of the two hemispheres as well as STN and PFC. This synchronization happens around the 4 Hz frequency and is stronger in bilateral STN comparing to STN Vs. PFC.

To go one step closer towards closed-loop DBS, an asynchronous detection method is proposed to detect self-driven finger movements. The time-frequency features of single channel LFP data did not have enough information for asynchronous detection. Therefore, a method based on temporal connectivity of STN between left and right hemispheres was proposed that was able to reach an acceptable performance for most of the subjects. We used a nonlinear regression method to measure this connectivity. Using templates matching we picked up temporal connectivity patterns and using thresholding, we were able to detect event and nonevent timings.

6.2 Discussion and Future Work

The computational complexity of the classification method explained in Chapter 4 is higher than the capability of the current devices. This is due to the high computational burden of calculating continuous wavelet coefficients as well as high number of features. However with the current state-of-the-art technology most of the computations can be performed in a server and the device is only responsible for recording, low level preprocessing and data packeting. The asynchronous detection method explained in Chapter 5 on the other can be implemented on a regular embedded device. This is because the algorithm uses only time domain features and can be implemented mainly by matrix multiplications.

Although the phase synchronization method explained in Chapter 3 is a powerful technique for studying the temporal connectivities, it is not useful for asynchronous detection. Calculating PLVs requires averaging the phase differences over the trials which means we need to have all the trials to be able to average them and also we need to have the trial onsets to align them for averaging. Therefore phase synchronization is not a practical technique for asynchronous real time detection and that's why we migrated towards nonlinear regression.

The proposed asynchronous algorithm is able to individually detect button pressing tasks. However a real-time closed-loop DBS algorithm is mostly involved with long periods of activity. For example, in the case of button pressing, the closed-loop DBS algorithm should be able to adjust the DBS parameters when the patient is typing in a laptop computer for minutes. This requires a higher level of decision making that decides based on several occurrences of a certain activity. This can increase the performance of the system because the system might miss some trials but still decide on occurrence of a task. Moving forward with designing the higher levels of decision making however requires a higher understanding of the next step (i.e. mapping the tasks into DBS parameters). In other words, we need to more specifically characterize the categories of activities that need to be distinguished and then design the higher level decision making techniques. For instance we might need the same DBS parameters for writing and speech tasks, therefore there is no need to distinguish between these two behaviors and they fall in the same category and they require the same decision making strategy.

The next step of designing the behavioral closed-loop systems is finding a mapping between activities and optimum DBS parameters. As we go forward with this step, more understanding of the nature of detected behaviors and their varieties will be achieved and we can adapt the current detection and classification methods to improve the performance

of the whole system. This work is an initial step towards such closed-loop systems and will be a starting point for more researches on using the BCI concept for deep brain stimulation.

The idea of using the connectivity of different tasks for event detection and classification is not limited only to closed-loop DBS. This idea can be applied to variety of BCI problems specially EEG signals that provide an extremely higher spatial variety. Also the fact that LFP data contain enough information for classification and even event detection can be a starting point for many closed-loop algorithm to move towards the recordings of the DBS device instead of external electrodes and sensors.

Bibliography

[1] Michael S Okun, Bruno V Gallo, George Mandybur, Jonathan Jagid, Kelly D Foote, Fredy J Revilla, Ron Alterman, Joseph Jankovic, Richard Simpson, Fred Junn, et al. Subthalamic deep brain stimulation with a constant-current device in parkinson's disease: an open-label randomised controlled trial. *The Lancet Neurology*, 11(2):140–149, 2012.

[2] 2013. URL "http://multimediacapsule.thomsonone.com/medtronic/new-medtronic-deep-brain-stimulation-system-the-first-to--sense-and-record-brain-ac

[3] Adam O Hebb, Felix Darvas, and Kai J Miller. Transient and state modulation of beta power in human subthalamic nucleus during speech production and finger movement. *Neuroscience*, 202:218–233, 2012.

[4] Theresa McClain Robert A Hauser. Coauthor(s): Rajesh Pahwa, Kelly E Lyons, 2010. URL "http://commons.wikimedia.org/wiki/File:Basal_ganglia_circuits.png".

[5] Adam O Hebb, Jun Jason Zhang, Mohammad H Mahoor, Christos Tsiokos, Charles Matlack, Howard Jay Chizeck, and Nader Pouratian. Creating the feedback loop: closed-loop neurostimulation. *Neurosurgery Clinics of North America*, 25(1):187–204, 2014.

[6] Maya Mendoza, 2013. URL "http://www.zenlama.com/the-difinitive-guide-to-increasing-you-mind-power".

[7] Pascal Fries. A mechanism for cognitive dynamics: neuronal communication through neuronal coherence. *Trends in cognitive sciences*, 9(10):474–480, 2005.

[8] AM Chandrasekhar and K Raghuveer. Intrusion detection technique by using k-means, fuzzy neural network and svm classifiers. In *Computer Communication and Informatics (ICCCI), 2013 International Conference on*, pages 1–7. IEEE, 2013.

[9] Julian M Fearnley and Andrew J Lees. Ageing and parkinson's disease: substantia nigra regional selectivity. *Brain*, 114(5):2283–2301, 1991.

[10] Curt R Freed, Paul E Greene, Robert E Breeze, Wei-Yann Tsai, William DuMouchel, Richard Kao, Sandra Dillon, Howard Winfield, Sharon Culver, John Q Trojanowski, et al. Transplantation of embryonic dopamine neurons for severe parkinson's disease. *New England Journal of Medicine*, 344(10):710–719, 2001.

[11] JP Hubble, KL Busenbark, S Wilkinson, RD Penn, K Lyons, and WC Koller. Deep brain stimulation for essential tremor. *Neurology*, 46(4):1150–1153, 1996.

[12] Puneet Plaha, Nikunj K Patel, and Steven S Gill. Stimulation of the subthalamic region for essential tremor. *Journal of neurosurgery*, 101(1):48–54, 2004.

[13] Joachim K Krauss, John Yianni, Thomas J Loher, and Tipu Z Aziz. Deep brain stimulation for dystonia. *Journal of Clinical Neurophysiology*, 21(1):18–30, 2004.

[14] Marie Vidailhet, Marie-France Jutras, David Grabli, and Emmanuel Roze. Deep brain stimulation for dystonia. *Journal of Neurology, Neurosurgery & Psychiatry*, pages jnnp–2011, 2012.

[15] Thomas Foltynie, Ludvic Zrinzo, Irene Martinez-Torres, Elina Tripoliti, Erika Petersen, Etienne Holl, Iciar Aviles-Olmos, Marjan Jahanshahi, Marwan Hariz, and Patricia Limousin. Mri-guided stn dbs in parkinson's disease without microelectrode recording: efficacy and safety. *Journal of Neurology, Neurosurgery & Psychiatry*, 82(4):358–363, 2011.

[16] Ji Yeoun Lee, Jin Wook Kim, Jee-Young Lee, Yong Hoon Lim, Cheolyoung Kim, Dong Gyu Kim, Beom Seok Jeon, and Sun Ha Paek. Is mri a reliable tool to locate the electrode after deep brain stimulation surgery? comparison study of ct and mri for the localization of electrodes after dbs. *Acta neurochirurgica*, 152(12):2029–2036, 2010.

[17] Marwan I Hariz. Complications of deep brain stimulation surgery. *Movement disorders*, 17(S3):S162–S166, 2002.

[18] H Russmann, J Ghika, P Combrement, JG Villemure, J Bogousslavsky, PR Burkhard, and FJG Vingerhoets. L-dopa-induced dyskinesia improvement after stn-dbs depends upon medication reduction. *Neurology*, 63(1):153–155, 2004.

[19] Jae-Hyeok Heo, Kyoung-Min Lee, Sun Ha Paek, Min-Jeong Kim, Jee-Young Lee, Ji-Young Kim, Soo-Young Cho, Yong Hoon Lim, Mi-Ryoung Kim, Soo Yeon Jeong, et al. The effects of bilateral subthalamic nucleus deep brain stimulation (stn dbs) on cognition in parkinson disease. *Journal of the neurological sciences*, 273(1):19–24, 2008.

[20] Helen S Mayberg, Andres M Lozano, Valerie Voon, Heather E McNeely, David Seminowicz, Clement Hamani, Jason M Schwalb, and Sidney H Kennedy. Deep brain stimulation for treatment-resistant depression. *Neuron*, 45(5):651–660, 2005.

[21] Jon López-Azcárate, Mikel Tainta, María C Rodríguez-Oroz, Miguel Valencia, Rafael González, Jorge Guridi, Jorge Iriarte, José A Obeso, Julio Artieda, and Manuel Alegre. Coupling between beta and high-frequency activity in the human subthalamic nucleus may be a pathophysiological mechanism in parkinson's disease. *The Journal of neuroscience*, 30(19):6667–6677, 2010.

[22] James C Houk, Joel L Davis, and David G Beiser. *Models of information processing in the basal ganglia*. MIT press, 1995.

[23] Peter Watson and Erwin B Montgomery. The relationship of neuronal activity within the sensori-motor region of the subthalamic nucleus to speech. *Brain and language*, 97 (2):233–240, 2006.

[24] Félix-Etienne François-Brosseau, Kristina Martinu, Antonio P Strafella, Michael Petrides, France Simard, and Oury Monchi. Basal ganglia and frontal involvement in self-generated and externally-triggered finger movements in the dominant and non-dominant hand. *European Journal of Neuroscience*, 29(6):1277–1286, 2009.

[25] Andrea A Kühn, Florian Kempf, Christof Brücke, Louise Gaynor Doyle, Irene Martinez-Torres, Alek Pogosyan, Thomas Trottenberg, Andreas Kupsch, Gerd-Helge Schneider, Marwan I Hariz, et al. High-frequency stimulation of the subthalamic nucleus suppresses oscillatory β activity in patients with parkinson's disease in parallel with improvement in motor performance. *The Journal of neuroscience*, 28(24):6165–6173, 2008.

[26] G Foffani, AM Bianchi, G Baselli, and A Priori. Movement-related frequency modulation of beta oscillatory activity in the human subthalamic nucleus. *The Journal of physiology*, 568(2):699–711, 2005.

[27] Andrea A Kühn, David Williams, Andreas Kupsch, Patricia Limousin, Marwan Hariz, Gerd-Helge Schneider, Kielan Yarrow, and Peter Brown. Event-related beta desynchronization in human subthalamic nucleus correlates with motor performance. *Brain*, 127(4):735–746, 2004.

[28] Eric Jacobsen and Richard Lyons. The sliding dft. *Signal Processing Magazine, IEEE*, 20(2):74–80, 2003.

[29] Charles K Chui and Ewald Quak. Wavelets on a bounded interval. In *Numerical Methods in Approximation Theory, vol. 9*, pages 53–75. Springer, 1992.

[30] Kok Keong Teo, Lipo Wang, and Zhiping Lin. Wavelet packet multi-layer perceptron for chaotic time series prediction: effects of weight initialization. In *Computational Science-ICCS 2001*, pages 310–317. Springer, 2001.

[31] Gyorgy Buzsaki. *Rhythms of the Brain*. Oxford University Press, 2006.

[32] Michel Le Van Quyen, Jack Foucher, Jean-Philippe Lachaux, Eugenio Rodriguez, Antoine Lutz, Jacques Martinerie, and Francisco J Varela. Comparison of hilbert transform and wavelet methods for the analysis of neuronal synchrony. *Journal of neuroscience methods*, 111(2):83–98, 2001.

[33] Flavio Fröhlich and David A McCormick. Endogenous electric fields may guide neocortical network activity. *Neuron*, 67(1):129–143, 2010.

[34] Juergen Fell and Nikolai Axmacher. The role of phase synchronization in memory processes. *Nature reviews neuroscience*, 12(2):105–118, 2011.

[35] N Kopell, GB Ermentrout, MA Whittington, and RD Traub. Gamma rhythms and beta rhythms have different synchronization properties. *Proceedings of the National Academy of Sciences*, 97(4):1867–1872, 2000.

[36] Paul HE Tiesinga, Jean-Marc Fellous, Jorge V José, and Terrence J Sejnowski. Computational model of carbachol-induced delta, theta, and gamma oscillations in the hippocampus. *Hippocampus*, 11(3):251–274, 2001.

[37] TR Burchell, HJ Faulkner, and MA Whittington. Gamma frequency oscillations gate temporally coded afferent inputs in the rat hippocampal slice. *Neuroscience letters*, 255(3):151–154, 1998.

[38] M Volgushev, M Chistiakova, and W Singer. Modification of discharge patterns of neocortical neurons by induced oscillations of the membrane potential. *Neuroscience*, 83(1):15–25, 1998.

[39] Pascal Fries, Pieter R Roelfsema, Andreas K Engel, Peter König, and Wolf Singer. Synchronization of oscillatory responses in visual cortex correlates with perception in interocular rivalry. *Proceedings of the National Academy of Sciences*, 94(23):12699–12704, 1997.

[40] Wolfgang Klimesch, Roman Freunberger, Paul Sauseng, and Walter Gruber. A short review of slow phase synchronization and memory: evidence for control processes in different memory systems? *Brain research*, 1235:31–44, 2008.

[41] Florian Mormann, Klaus Lehnertz, Peter David, and Christian E Elger. Mean phase coherence as a measure for phase synchronization and its application to the eeg of epilepsy patients. *Physica D: Nonlinear Phenomena*, 144(3):358–369, 2000.

[42] Ron Levy, William D Hutchison, Andres M Lozano, and Jonathan O Dostrovsky. High-frequency synchronization of neuronal activity in the subthalamic nucleus of parkinsonian patients with limb tremor. *The Journal of neuroscience*, 20(20):7766–7775, 2000.

[43] Felix Darvas and Adam O Hebb. Task specific inter-hemispheric coupling in human subthalamic nuclei. *Frontiers in human neuroscience*, 8, 2014.

[44] Michael Rosenblum, Arkady Pikovsky, Jürgen Kurths, Carsten Schäfer, and Peter A Tass. Phase synchronization: from theory to data analysis. *Handbook of biological physics*, 4(279-321):93–94, 2001.

[45] Jean-Philippe Lachaux, Eugenio Rodriguez, Jacques Martinerie, Francisco J Varela, et al. Measuring phase synchrony in brain signals. *Human brain mapping*, 8(4):194–208, 1999.

[46] Alan V Oppenheim, Ronald W Schafer, John R Buck, et al. *Discrete-time signal processing*, volume 2. Prentice-hall Englewood Cliffs, 1989.

[47] Julius O Smith. *Mathematics of the discrete Fourier transform (DFT): with audio applicaitons*. Julius Smith, 2007.

[48] Alejo J Nevado Holgado, John R Terry, and Rafal Bogacz. Conditions for the generation of beta oscillations in the subthalamic nucleus–globus pallidus network. *The Journal of Neuroscience*, 30(37):12340–12352, 2010.

[49] Andreas K Engel, Christian KE Moll, Itzhak Fried, and George A Ojemann. Invasive recordings from the human brain: clinical insights and beyond. *Nature Reviews Neuroscience*, 6(1):35–47, 2005.

[50] Kai J Miller, Gerwin Schalk, Eberhard E Fetz, Marcel den Nijs, Jeffrey G Ojemann, and Rajesh PN Rao. Cortical activity during motor execution, motor imagery, and imagery-based online feedback. *Proceedings of the National Academy of Sciences*, 107 (9):4430–4435, 2010.

[51] Florian Kempf, Andrea A Kühn, Andreas Kupsch, Christof Brücke, Lutz Weise, Gerd-Helge Schneider, and Peter Brown. Premovement activities in the subthalamic area of patients with parkinson's disease and their dependence on task. *European Journal of Neuroscience*, 25(10):3137–3145, 2007.

[52] Ian Jolliffe. *Principal component analysis*. Wiley Online Library, 2005.

[53] Corinna Cortes and Vladimir Vapnik. Support-vector networks. *Machine learning*, 20 (3):273–297, 1995.

[54] Fabien Lotte, Marco Congedo, Anatole Lécuyer, Fabrice Lamarche, Bruno Arnaldi, et al. A review of classification algorithms for eeg-based brain–computer interfaces. *Journal of neural engineering*, 4, 2007.

[55] Richard O Duda, Peter E Hart, and David G Stork. *Pattern classification*. John Wiley & Sons, 2012.

[56] Chih-Chung Chang and Chih-Jen Lin. Libsvm: a library for support vector machines. *ACM Transactions on Intelligent Systems and Technology (TIST)*, 2(3):27, 2011.

[57] Kevin Beyer, Jonathan Goldstein, Raghu Ramakrishnan, and Uri Shaft. When is nearest neighbor meaningful? In *Database TheoryICDT99*, pages 217–235. Springer, 1999.

[58] Chih-Wei Hsu, Chih-Chung Chang, Chih-Jen Lin, et al. A practical guide to support vector classification, 2003.

[59] Bashar Awwad Shiekh Hasan and John Q Gan. Temporal modeling of eeg during self-paced hand movement and its application in onset detection. *Journal of neural engineering*, 8(5):056015, 2011.

[60] Bashar Awwad Shiekh Hasan and John Q Gan. Unsupervised movement onset detection from eeg recorded during self-paced real hand movement. *Medical & biological engineering & computing*, 48(3):245–253, 2010.

[61] Catherine Marie Sweeney-Reed and Slawomir Jaroslaw Nasuto. Detection of neural correlates of self-paced motor activity using empirical mode decomposition phase locking analysis. *Journal of neuroscience methods*, 184(1):54–70, 2009.

[62] Eileen Lew, Ricardo Chavarriaga, Stefano Silvoni, and José del R Millán. Detection of self-paced reaching movement intention from eeg signals. *Front. Neuroeng*, 5(13), 2012.

[63] Dandan Huang, Peter Lin, Ding-Yu Fei, Xuedong Chen, and Ou Bai. Decoding human motor activity from eeg single trials for a discrete two-dimensional cursor control. *Journal of neural engineering*, 6(4):046005, 2009.

[64] Mads Jochumsen, Imran Khan Niazi, Natalie Mrachacz-Kersting, Dario Farina, and Kim Dremstrup. Detection and classification of movement-related cortical potentials associated with task force and speed. *Journal of neural engineering*, 10(5):056015, 2013.

[65] Imran Khan Niazi, Ning Jiang, Olivier Tiberghien, Jørgen Feldbæk Nielsen, Kim Dremstrup, and Dario Farina. Detection of movement intention from single-trial movement-related cortical potentials. *Journal of neural engineering*, 8(6):066009, 2011.

[66] Bernhard Graimann, Jane E Huggins, A Schlogl, Simon P Levine, and Gert Pfurtscheller. Detection of movement-related patterns in ongoing single-channel electrocorticogram. *Neural Systems and Rehabilitation Engineering, IEEE Transactions on*, 11(3):276–281, 2003.

[67] Zuoguan Wang, Aysegul Gunduz, Peter Brunner, Anthony L Ritaccio, Qiang Ji, and Gerwin Schalk. Decoding onset and direction of movements using electrocorticographic (ecog) signals in humans. *Frontiers in neuroengineering*, 5, 2012.

[68] Tobias Pistohl, Thomas Sebastian Benedikt Schmidt, Tonio Ball, Andreas Schulze-Bonhage, Ad Aertsen, and Carsten Mehring. Grasp detection from human ecog during natural reach-to-grasp movements. *PloS one*, 8(1):e54658, 2013.

[69] Omid Talakoub, Milos R Popovic, Jessie Navaro, Clement Hamani, Erich T Fonoff, and Willy Wong. Temporal alignment of electrocorticographic recordings for upper limb movement. *Frontiers in Neuroscience*, 8:431, 2015.

[70] Nicolas Y Masse, Beata Jarosiewicz, John D Simeral, Daniel Bacher, Sergey D Stavisky, Sydney S Cash, Erin M Oakley, Etsub Berhanu, Emad Eskandar, Gerhard Friehs, et al. Reprint of non-causal spike filtering improves decoding of movement intention for intracortical bcis. *Journal of neuroscience methods*, 244:94–103, 2015.

[71] Joshua Egan, Justin Baker, Paul House, and Bradley Greger. Detection and classification of multiple finger movements using a chronically implanted utah electrode array. In *Engineering in Medicine and Biology Society, EMBC, 2011 Annual International Conference of the IEEE*, pages 7320–7323. IEEE, 2011.

[72] Michael Mace, Nada Yousif, Mohammad Naushahi, Khondaker Abdullah-Al-Mamun, Shouyan Wang, Dipankar Nandi, and Ravi Vaidyanathan. An automated approach towards detecting complex behaviours in deep brain oscillations. *Journal of neuroscience methods*, 224:66–78, 2014.

[73] Soroush Niketeghad, Adam O Hebb, Joshua Nedrud, Sara J Hanrahan, and Mohammad H Mahoor. Single trial behavioral task classification using subthalamic nucleus

local field potential signals. In *Engineering in Medicine and Biology Society (EMBC), 2014 36th Annual International Conference of the IEEE*, pages 3793–3796. IEEE, 2014.

[74] PL Nunez. Methods to estimate spatial properties of dynamic cortical source activity. *Functional brain imaging*, pages 3–10, 1988.

[75] Fernando Lopes da Silva, Jan Pieter Pijn, and Peter Boeijinga. Interdependence of eeg signals: linear vs. nonlinear associations and the significance of time delays and phase shifts. *Brain topography*, 2(1-2):9–18, 1989.

[76] Douglas M Bates and Donald G Watts. *Nonlinear regression: iterative estimation and linear approximations*. Wiley Online Library, 1988.

[77] F Wendling, F Bartolomei, JJ Bellanger, and P Chauvel. Interpretation of interdependencies in epileptic signals using a macroscopic physiological model of the eeg. *Clinical neurophysiology*, 112(7):1201–1218, 2001.

[78] Alexander Kraskov, Harald Stögbauer, and Peter Grassberger. Estimating mutual information. *Physical review E*, 69(6):066138, 2004.

[79] J Arnhold, P Grassberger, K Lehnertz, and CE Elger. A robust method for detecting interdependences: application to intracranially recorded eeg. *Physica D: Nonlinear Phenomena*, 134(4):419–430, 1999.

[80] Francisco Varela, Jean-Philippe Lachaux, Eugenio Rodriguez, and Jacques Martinerie. The brainweb: phase synchronization and large-scale integration. *Nature reviews neuroscience*, 2(4):229–239, 2001.

[81] Rangaraj M Rangayyan et al. *Biomedical signal analysis*. IEEE Standards Office, 2001.

[82] Tom Fawcett. An introduction to roc analysis. *Pattern recognition letters*, 27(8): 861–874, 2006.

[83] Ian Jolliffe. *Principal component analysis*. Wiley Online Library, 2002.

Conditional Variance

The conditional variance of $Y[n+\tau]$ given $X[n]$ where τ is the amount of time delay applied on signal Y is calculated as follows:

1. Normalize $X[n]$ and $Y[n+\tau]$.

2. Assuming $X[n]$ and $Y[n+\tau]$ have the same length, map every time point n^* to a 2-D space where $x^* = X[n^*]$ and $y^* = Y[n^* + \tau]$ are the coordinates.

3. Divide the space in identical vertical bins $B = \{b_1, b_2, , b_k\}$ based on their x value.

4. The center of the bin b_i is defined as $c_i = (x_{c_i}, y_{c_i})$ where x_{c_i} is the mean of x values of lower and higher bin band and y_{c_i} is the mean of y values of the points that fall into the b_i.

5. Connect the centers to obtain a regression function $y = f(x)$.

6. Calculate the conditional variance from the following:

$$VAR(Y[n+\tau]|X[n]) = \frac{1}{N}\sum_{i=1}^{N}(y_i - f(x_i))^2 \tag{1}$$

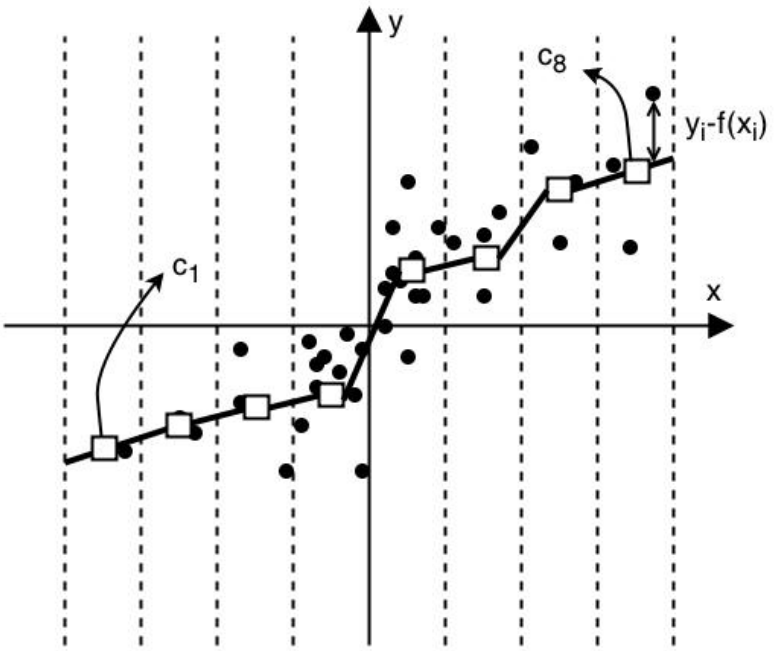

FIGURE 1: Regression function estimated from the points corresponding to the 2-channel data.

Component selection

The correlation coefficients $h^{2*}_{X_iY_j}[n]$ corresponding to every possible bilateral pair are calculated from the training data. Let's say $i, j = 1, ..., N_{ch}$ where N_{ch} is the number of bilateral channels for each side. Therefore ${N_{ch}}^2$ possible normalized correlation coefficients are produced. The PCA is applied to the resulting timeseries to obtain $N_c h^2$ components $c^{2*}_{(XY)_k}[n]$ $(k = 1, ..., {N_{ch}}^2)$ [83]. A template for all of the components is created and the template matching algorithm is applied on each component. This results in normalized correlation coefficients $\gamma^{2*}_{XY_k}[n]$ that are used to detect events and create ROC curves. Area under curve (AUC) for all the ROC curves is calculated and the component corresponding to the highest AUC, $c^{2*}_{(XY)_k}[n]$ is selected as the optimum component. $c^{2*}_{(XY)_k}[n]$ is a linear combination of all the correlation coefficients $h^{2*}_{X_iY_j}[n]$:

$$c^{2*}_{(XY)_k}[n] = \sum_{k=1}^{{N_{ch}}^2} \lambda^*_k h^{2*}_{X_iY_j}[n] \tag{2}$$

where λ^*_k are the optimum component coefficients and are used in the system to create the optimum component.